Geochemistry 83 (2023) 126004

Contents lists available at ScienceDirect

Geochemistry

journal homepage: www.elsevier.com/locate/chemer

Invited review

Early solar system chronology from short-lived chronometers

Aryavart Anand [a,b,*], Klaus Mezger [b]

[a] Max-Planck-Institut für Sonnensystemforschung, Justus-von-Liebig-Weg 3, 37077 Göttingen, Germany
[b] Institut für Geologie, Universität Bern, Baltzerstrasse 1+3, 3012 Bern, Switzerland

ARTICLE INFO

Handling Editor: Astrid Holzheid

Keywords:
Early solar system
Chronology
Planetesimal accretion
Meteorites
Short-lived isotopes
Planetesimal differentiation
Chondrites
Core formation

ABSTRACT

Age constraints on early solar system processes and events can be derived from meteorites and their components using different radioisotope systems. Due to the short time interval from the first formation of solids in the solar nebula to the accretion and differentiation of planetesimals and some planets, a high temporal resolution of the chronometers is essential and can be obtained in most cases only with short-lived isotope systems, particularly the decay schemes ^{26}Al-^{26}Mg, ^{182}Hf-^{182}W and ^{53}Mn-^{53}Cr. These chronometers provide highly resolved time constrains for the formation of the first solids (Ca-Al-rich inclusions or CAIs), chondrules, planetary cores, for the accretion and differentiation of planetesimals and hydrous/thermal alteration. Formation of Ca-Al-rich inclusions was restricted to the inner solar system and to a short time interval of ≪1 Ma, and marks the "beginning of the solar system". It was immediately followed by planetesimal formation. The oldest planetesimals accreted within a few 10^5 a after the formation of CAIs. The accretion of early formed planetesimals and their subsequent differentiation into a metallic core and a silicate mantle was a continuous process that occurred at different times in different locations of the solar nebula and extended over a time interval of at least ~4 Ma. During this time interval the accretion process may have changed from planetesimal formation via streaming instability to pebble accretion. The earliest formed bodies that still needed to settle into stable orbits could have created bow shocks in the adjacent regions still composed of dust and gas which resulted in the formation of silicate chondrules in a narrow time interval from 1.8 to 3 Ma. The chondrule forming interval was immediately followed by the accretion of the chondrite parent bodies, which did not differentiate due to their late accretion when most of the heat producing ^{26}Al had already decayed. Thus, the chondrite parent bodies are a second generation of planetesimals, but chemically they are the most primitive material preserved from the early solar system. Aqueous alteration of volatile rich planetesimals peaked at ca. 3.5 Ma and coincided with metamorphism recorded in ordinary chondrite parent bodies. The compilation of ages from different meteorites and their components demonstrates that similar accretion and differentiation processes do not follow an identical time line from dust to planetesimal formation and they do not correlate with the location in the disk. The accretion of matter into planetesimals was a local phenomenon with stochastic spatial distribution. The spatial distribution of accretion processes operating in the early solar system appears to be similar to those in some directly observable nascent exo-planetary systems.

1. Introduction

Following the discovery of exoplanets and whole exoplanetary systems, the study of the processes in the early solar system and their timing has received enhanced attention. One goal of these studies of exoplanetary systems is the derivation of a model that describes the path from the collapse of a molecular cloud to the formation of a multi-planetary solar system. Such a universal and unifying model will have to have our solar system as one possible outcome. The solar system is currently the only planetary system for which it is possible to study different pre-planetary and planetary materials directly through the analysis of actual material delivered to Earth as meteorites, via space missions that perform in-situ analyses or via laboratory analysis on samples returned to Earth. All these studies provide key chemical and isotopic data that inform on the formation and evolution of planetary bodies of different sizes and with possibly different evolution paths. A key parameter in these studies is the timing of the different processes from the formation of the first solids to the final accretion and differentiation of

* Corresponding author at: Max-Planck-Institut für Sonnensystemforschung, Justus-von-Liebig-Weg 3, 37077 Göttingen, Germany.
E-mail addresses: anand@mps.mpg.de (A. Anand), klaus.mezger@unibe.ch (K. Mezger).

https://doi.org/10.1016/j.chemer.2023.126004
Received 27 February 2023; Received in revised form 28 May 2023; Accepted 29 May 2023
Available online 30 May 2023

planetesimals and planets. This time information can be used to discriminate among different proposed scenarios that may be applicable to early solar system processes and events. Subsequently, this information can be used in physical models to constrain possible scenarios for planet formation and make predictions about exo-planetary systems.

A number of short-lived radionuclides were extant at the beginning of the solar system. Their existence has been documented through excesses in daughter isotopes in meteorites and their components. The abundances of these isotopes had a significant impact on early solar processes including the timing of stellar nucleosynthesis events prior to the formation of the solar system, heating of early-formed planetesimals and chronology of events in the early solar system. The significant advancements in the analytical techniques in the past two decades to measure isotope abundances with high precision and accuracy have led to tighter constraints on the initial abundances of the short-lived radionuclides and hence in their application in detailed and highly resolved chronological studies. This review outlines and puts in sequence, the timing of different physical and chemical processes that occurred in the early solar system and on the early accreted planetesimals that existed during the nebula stage, using multiple short-lived chronometers.

In general, radionuclides can be used to date element fractionation. Thus, in principle any process that separates the parent from the daughter element can be dated. This is done via isochrons for long-lived radionuclides or pseudo-isochrons/model ages using extinct or short-lived radionuclides. In order to obtain high precision ages, element fractionation should be large. Materials are selected that preserve isotope compositions at the time of formation, i.e., parent/daughter fractionation. Short-lived radionuclide systems can provide ages for mineral formation during condensation from the solar nebula, crystallization of a melt, metal-silicate separation in a molten system leading to core formation, onset and duration of metamorphism on parent bodies, aqueous alteration and cooling histories of planetesimals. Dating meteorite samples or their components first requires the identification of the process or event that should be dated and then the selection of material that records the process or event that caused at the same time separation of a radioactive parent element from the daughter element. Since the time resolution necessary to resolve early solar system processes is on the scale of a few Ma out of 4.57 Ga for the whole solar system, high-resolution chronometers are essential. Most long-lived isotope systems provide absolute ages with uncertainties of a few % (e.g., ^{87}Rb-^{87}Sr, ^{147}Sm-^{143}Nd, ^{176}Lu-^{176}Hf, ^{40}K-^{40}Ar-^{40}Ca, ^{187}Re-^{187}Os), with the exception of the U-Pb system that can achieve 0.05 % under favourable conditions (e.g., Amelin, 2006; Bollard et al., 2017, 2019). However, rapid decay of short-lived isotopes (whose parent isotopes are now essentially extinct) results in significant isotopic variations on very short timescales. Hence, the short-lived chronometers have the resolving power to constrain the timing of key processes during the very first few Ma of the solar system from the time of mineral condensation to the formation and differentiation of planetary bodies. Studying the very first few Ma of the solar system with high temporal resolution is essential to reconstruct how it came into existence and how its planets formed. The sequence of differentiation and accretion in time and space during the first few Ma set the stage and controlled the architecture of the solar system with its different planets and their distinct chemical composition. Short-lived isotopes provide the necessary time information for the different fractionation processes during the earliest and critical stages of solar system evolution.

1.1. Dating with the short-lived isotope systems

For short-lived isotope systems to yield useful dates for events and processes during the first ca. 5 Ma of the solar system, it is necessary that the parent isotope has a sufficient abundance to produce well measurable amounts of daughter isotope, parent and daughter element have to fractionate appreciably during the process that is to be dated and the half-life of the parent isotope needs to be well known and is ideally between 0.5 and 10 Ma. Table 1 lists the short-lived isotope systems that have been realized to date. The origin and abundance of short-lived radionuclides are discussed in the recent review by Davis (2022). Many of the short-lived systems listed in Table 1 are regularly used as chronometers in meteorites and their components to obtain precise and accurate ages for processes and events in the early solar system.

The fundamentals on how ages can be obtained using an isotope system with a short-lived parent isotope are given in White (2023). It involves the construction of an isochron based on at least two data points (samples). Similar to the long-lived isotope chronometers, the excess of the radiogenic daughter isotope correlates with the concentration of the parent isotope in the sample. The slope of the correlation line gives the abundance of the parent isotope at the time of fractionation of the different samples. In order to translate this into an age it is essential to know the abundance of the parent isotope at a given point in time, which is determined using an absolute age as an anchor. For this purpose, the most suitable isotope system is the U-Pb system, because it can yield high precision ages for old samples, like meteorites (e.g. Amelin, 2006). Thus, all ages determined with short-lived isotopes are "anchored" to at least one sample with a highly precise absolute age. Apart from having been dated with an absolute chronometer, any viable anchor needs to satisfy the following conditions: (1) diverse mineral composition to enable the adequate fractionation of parent-daughter element ratios for a range of isotope systems, (2) rapid cooling to enable multiple isotopic systems to close within their given resolution without subsequent partial re-equilibration events, (3) secondary processes that disturb isotopic systems must be absent or insignificant (Sanborn et al., 2019). Usually, angrites such as D'Orbigny, Lewis Cliff (LEW) 86010 and Angra dos Reis are considered to be nearly ideal anchors, however, recent studies of ancient ungrouped achondrites such as Northwest Africa (NWA) 6704 and Erg Chech (EC) 002, dated by multiple isotope systematics are proving to be promising anchors as well (Sanborn et al., 2019; Barrat et al., 2021; Fang et al., 2022; Anand et al., 2022). Some differences in ages reported for meteorites or their components can be related to different anchors used and thus need to be adjusted to enable comparison.

It is important to consider what event is being recorded by an isochron. For an 'internal isochron' different phases (e.g. minerals, mesostasis) from a coherent sample are analyzed and this yields the time of fractionation corresponding to the formation of individual phases within this sample. It is assumed that the different phases did not experience element exchange after formation and thus isotopic closure is instantaneous (or near-instantaneous) and maintained until the time of dating. For an 'external isochron' different bulk samples are analyzed that are thought to have formed from a common reservoir. The age obtained then corresponds to the time of fractionation that occurred in this common reservoir.

For instance, the ^{26}Al-^{26}Mg studies on chondrule formation focus on chondrules from unequilibrated chondrites containing primary plagioclase or glass as the main mesostasis phase. The plagioclase and glass occur as primary products of melt and have high Al/Mg and hence excess radiogenic ^{26}Mg, if they formed at a time when ^{26}Al was still extant. A ^{26}Al-^{26}Mg 'internal isochron' can be determined on a single chondrule level by measuring the δ^{26}Mg (deviation from terrestrial ^{26}Mg/^{24}Mg in parts 10^3) and ^{27}Al/^{24}Mg in individual minerals within the chondrule. The excess ^{26}Mg is measured using an ion microprobe and reported as δ^{26}Mg, i.e., deviation from terrestrial ^{26}Mg/^{24}Mg in parts of 10^3. A positive correlation between δ^{26}Mg and ^{27}Al/^{24}Mg indicates in situ decay of ^{26}Al. The slope of this isochron yields the initial $(^{26}Al/^{27}Al)_0$ ratio at the last time the sample crystallized and the diffusive exchange of parent and daughter elements among the different minerals stopped. The initial $(^{26}Al/^{27}Al)_0$ ratio, when anchored to the initial $(^{26}Al/^{27}Al)_0$ of the D'Orbigny angrite, gives the time of chondrule formation relative to the formation age of D'Orbigny. Subsequently, the relative age can be translated into an absolute age using the U-isotope

Table 1
Summary of short-lived isotope systems including the initial abundances of the radionuclides at the beginning of the solar system (Davis, 2022) and the materials used to obtain chronometric information.

Fractionation	Parent nuclide	Half-life (Ma)	Daughter nuclide	Estimated initial solar system abundance	Identified in	Ref.
Nebular	^{7}Be	53.22 ± 0.06 d[a]	^{7}Li	(6.1 ± 1.3) × 10^{-3} × ^{9}Be	CAIs	1
Nebular	^{10}Be	1.3870 ± 0.0012	^{10}B	(7.3 ± 1.7) × 10^{-4} × ^{9}Be	CAIs	2, 3
Nebular, planetary	^{27}Al	0.717 ± 0.024	^{26}Mg	(5.20 ± 0.13) × 10^{-5} × ^{27}Al	CAIs, chondrules, achondrites	4, 5
Planetary	^{36}Cl	0.3013 ± 0.0015	^{36}S, ^{36}Ar	(1.7–3.0) × 10^{-5} × ^{35}Cl	CAIs, chondrites	6
Nebular	^{41}Ca	0.0994 ± 0.0015	^{41}K	4 × 10^{-9} × ^{40}Ca	CAIs	7
Nebular, planetary	^{53}Mn	3.7 ± 0.4	^{53}Cr	(7 ± 1) × 10^{-6} × ^{55}Mn	CAIs, chondrules, carbonates, achondrites	8
Nebular, planetary	^{60}Fe	2.62 ± 0.04	^{60}Ni	(1.01 ± 0.27) × 10^{-8} × ^{56}Fe	Achondrites, chondrites	9
Planetary	^{92}Nb	34.7 ± 2.4	^{92}Zr	(1.66 ± 0.10) × 10^{-5} × ^{93}Nb	Chondrites, mesosiderites	10
Planetary	^{97}Tc	<4.21 ± 0.16	^{97}Mo	1 × 10^{-6} × ^{92}Mo	Iron meteorites	11
Planetary	^{98}Tc	4.2 ± 0.3	^{98}Ru	<2 × 10^{-5} × ^{96}Ru	Iron meteorites	12
Planetary	^{107}Pd	6.5 ± 0.3	^{107}Ag	(5.9 ± 2.2) × 10^{-5} × ^{108}Pd	Iron meteorites, pallasites	13
Planetary	^{126}Sn	0.230 ± 0.014	^{126}Te	<3 × 10^{-6} × ^{124}Sn	Chondrules, secondary minerals	14
Planetary	^{129}I	16.14 ± 0.12	^{129}Xe	(1.35 ± 0.02) × 10^{-4} × ^{127}I	Chondrules, secondary minerals	3
Nebular	^{135}Cs	1.33 ± 0.19	^{135}Ba	<2.8 × 10^{-6} × ^{133}Cs	CAIs, chondrites	15
Planetary	^{146}Sm	103 ± 5[b]	^{142}Nd	(8.40 ± 0.32) × 10^{-3} × ^{144}Sm	Planetary differentiates	16
Planetary	^{182}Hf	8.90 ± 0.09	^{182}W	(1.018 ± 0.043) × 10^{-4} × ^{180}Hf	CAIs, planetary differentiates	17
Planetary	^{205}Pb	17.0 ± 0.9	^{205}Tl	(1.8 ± 1.2) × 10^{-3} × ^{204}Pb	Chondrites	18
Planetary	^{244}Pu	81.3 ± 0.3	^{232}Th; fission	(7.7 ± 0.6) × 10^{-3} × ^{238}U	CAIs, chondrites	19
Nebular	^{247}Cm	15.6 ± 0.5	^{235}U	(5.6 ± 0.3) × 10^{-3} × ^{235}U	CAIs	20, 6

Ref: (b) Friedman et al. (1966) and Meissner et al. (1987) (1) Chaussidon et al. (2006) (2) Dunham et al. (2022) (3) Davis (2022) (4) Jacobsen et al. (2008) (5) Wasserburg et al. (2012) (6) Tang et al. (2017) (7) Liu et al. (2012) (8) Tissot et al. (2017) (9) Tang and Dauphas (2015) (10) Haba et al. (2021) (11) Burkhardt et al. (2011) (12) Becker and Walker (2003) (13) Schönbächler et al. (2008) (14) Brennecka et al. (2017) (15) Brennecka and Kleine (2017) (16) Fang et al. (2022) (17) Kruijer et al. (2014a) (18) Palk et al. (2018) (19) Turner et al. (2007) (20) Tissot et al. (2016).

[a] Half-life for ^{7}Be in days (d).

corrected ^{207}Pb-^{206}Pb age of the D'Orbigny angrite (e.g., Hutcheon and Hutchison, 1989; Pape et al., 2019; Siron et al., 2021, 2022; Fukuda et al., 2022).

In addition to the isochron approach for dating, short-lived isotope systems can also be used to obtain precise and meaningful 'model ages' from a single mineral phase/fraction with a near-zero parent/daughter ratio. These model ages are inferred as the time at which the ingrowth of daughter isotope stopped, which could be a process that practically removed the parent radionuclide from this mineral phase/fraction. In the absence of the parent radionuclide, this mineral phase/fraction preserves the initial abundance of the radiogenic daughter isotope of its host material at the time of formation. A model age can be obtained by measuring the radiogenic daughter abundance of this mineral phase/fraction and comparing it to its evolution in a model or assumed reservoir (such as the chondritic reservoir) from which the sample presumably originated. Precise model ages can be obtained only for short-lived systems with abundant radioactive parent isotopes (see Table 1 for parent nuclide abundance) at time zero and where ingrowth over time is well beyond analytical uncertainties for daughter isotope ratio measurement. In case of a chondritic reservoir, the radiogenic ingrowth of ^{26}Mg is only 20 ppm, which makes it less suitable to obtain model ages using ^{26}Al-^{26}Mg system due to minimal ingrowth in comparison with the achievable analytical uncertainty of the ^{26}Mg isotope ratio measurement. However, the radiogenic ingrowths of ^{182}W and ^{53}Cr in the chondritic reservoir are ~150 ppm and ~70 ppm, respectively, which are well exceeding the current analytical uncertainties on ^{182}W and ^{53}Cr isotope measurements and hence, these systems are widely used for dating meteorites and meteorite components using the model age approach (e.g., Kleine et al., 2009; Anand et al., 2021a, 2021b).

1.2. Distribution of short-lived isotope systems in the solar system

An essential condition for the reliable application of short-lived isotope systems is the homogeneous distribution of the parent isotope within the reservoir from which samples are derived, which in the present case are the regions of the solar system from where meteorites or returned samples can be dated through isotope ratio measurements. If the distribution of short-lived isotopes in the solar system was strongly heterogeneous, then the parent/daughter isotope systematics of the material investigated would provide information that is a mixture of the time of parent/daughter element fractionation (=age of the sample) and the place in the solar system. In this case, to obtain robust age information, the abundance of the short-lived isotope needs to be known or determined for each parental reservoir for every sample.

Isotope heterogeneity among meteorites and their components is well documented for a variety of stable non-radiogenic isotopes originating from different nucleosynthetic sources that contributed to the matter in the solar system. These variations indicate at least two fundamentally different nebular source regions, which have been termed the non-carbonaceous (NC) and carbonaceous (CC) reservoirs (Warren, 2011; Budde et al., 2016a). The short-lived isotopes may have been delivered by at least one source that produced these isotopes shortly before addition to the solar nebula. The heterogeneity of stable non-radiogenic isotopes in and among meteorites is evidence that the solar nebula was not completely homogenized isotopically. Thus, it could be expected that this heterogeneity also applies to the short-lived radioactive isotopes. However, the variations of stable non-radiogenic isotopes are all less than a per mill. In order for heterogeneity in short-lived isotopes to have a detectable effect on the resulting age information, these heterogeneities have to be several percent, which is unlikely.

This issue of heterogeneity in parent isotope abundances has been discussed in many studies reporting ^{26}Al-^{26}Mg ages (e.g., Makide et al., 2011; Krot et al., 2012; Schiller et al., 2015) and comparing Pb-Pb ages of chondrules with their ^{26}Al-^{26}Mg ages (e.g., Bollard et al., 2019). The coherence of the Pb-Pb and ^{26}Al-^{26}Mg chronometers has been demonstrated recently by Reger et al. (2023) using high precision ages determined on the meteorite EC 002. Larsen et al. (2020) reported bulk CAI isochrons for CV and CR chondrites with similar slopes that are close to the canonical $(^{26}Al/^{27}Al)_0$ value but with different initial $(^{26}Mg/^{24}Mg)_0$. Davis (2022) emphasized that although this variable initial $(^{26}Mg/^{24}Mg)_0$ can be attributed to spatial heterogeneities in Mg isotopes, but the similar slope of the bulk CAI isochrons implies indistinguishable ^{26}Al abundances for the regions where CAIs originate from. In addition, the coherence of ages determined with different chronometers on the same materials (Section 2.2) also supports homogeneous distribution of the short-lived isotopes in the solar system given the currently achievable analytical uncertainties for isotope ratio measurements.

2. Chronology of the early solar system from short-lived isotope systems

2.1. Parameters

The following section provides a compilation of the literature data on the ^{26}Al-^{26}Mg, ^{182}Hf-^{182}W and ^{53}Mn-^{53}Cr chronology of the early solar system objects and processes. In order to make these published data internally consistent and thus comparable, it is essential to define the relevant parameters that are needed to derive ages, such as the initial abundance of the parent and daughter nuclides at the beginning of the solar system of any time thereafter. For this compilation, the initial $(^{26}Al/^{27}Al)_0$ ratios determined in the ^{26}Al-^{26}Mg systematics of the samples from different studies are anchored to the canonical $(^{26}Al/^{27}Al)_0$ of 5.23×10^{-5} and the relative ages are recalculated with this value. The canonical $(^{26}Al/^{27}Al)_0$ ratio is taken from Jacobsen et al. (2008) who determined it from an external isochron obtained using multiple bulk CAIs separated from the Allende meteorite. Similar to the ^{26}Al-^{26}Mg system, initial $(^{182}Hf/^{180}Hf)_0$ determined in the ^{182}Hf-^{182}W systematics of the samples from various studies are anchored to the canonical $(^{182}Hf/^{180}Hf)_0$ ratio of 1.018×10^{-4}. The canonical $(^{182}Hf/^{180}Hf)_0$ ratio was determined from an external isochron obtained using CAIs from the Allende, NWA 6870 and NWA 6717 CV3 chondrites (Kruijer et al., 2014a).

Unlike ^{26}Al-^{26}Mg and ^{182}Hf-^{182}W systems, determining initial $(^{53}Mn/^{55}Mn)_0$ values for CAIs has proven difficult due to the low abundance of Mn and Cr, which is a direct consequence of their volatility at high temperatures (Nyquist et al., 2009). Hence, initial $(^{53}Mn/^{55}Mn)_0$ values from ^{53}Mn-^{53}Cr systematics are generally anchored to angrites such as D'Orbigny and LEW 86010. However, for comparisons with the ^{26}Al-^{26}Mg and ^{182}Hf-^{182}W systems, the initial $(^{53}Mn/^{55}Mn)_0$ ratios determined from the ^{53}Mn-^{53}Cr systematics of the samples from different studies should also be anchored to a canonical $(^{53}Mn/^{55}Mn)_0$ ratio. Since the direct determination of the canonical $(^{53}Mn/^{55}Mn)_0$ from CAIs is not possible, the angrite D'Orbigny's initial $(^{53}Mn/^{55}Mn)_0$ ($=3.24 \pm 0.04 \times 10^{-6}$) and its U corrected Pb-Pb age (=4563.37 ± 0.25 Ma, Brennecka and Wadhwa, 2012) is calibrated against the Pb-Pb age of the CAIs (4567.30 ± 0.16 Ma, Connelly et al., 2012). This gives an indirect canonical $(^{53}Mn/^{55}Mn)_0$ value of 6.77×10^{-6}, which is then used in the following compilation as an anchor to recalculate the ages of the samples from their reported initial $(^{53}Mn/^{55}Mn)_0$ ratios.

The age of D'Orbigny based on its initial $(^{26}Al/^{27}Al)_0$ ($=3.98 \pm 0.39 \times 10^{-7}$, Spivak-Birndorf et al., 2009; Schiller et al., 2010a, 2015; Sanborn et al., 2019) anchored to the canonical $(^{26}Al/^{27}Al)_0$ ratio, is 4562.2 ± 0.2 Ma. Similarly, the age of D'Orbigny when its initial $(^{182}Hf/^{180}Hf)_0$ ($=7.15 \pm 0.17 \times 10^{-5}$, Kleine et al., 2012) is anchored to the canonical $(^{182}Hf/^{180}Hf)_0$ ratio is 4562.8 ± 0.6 Ma. Note that although the ^{26}Al-^{26}Mg and ^{182}Hf-^{182}W ages of D'Orbigny are consistent with each other, there is a disparity of 0.6–1 Ma with the U-corrected Pb-Pb age of D'Orbigny. The reason for this disparity is unclear at present and needs further ^{26}Al-^{26}Mg and ^{182}Hf-^{182}W investigation of the D'Orbigny angrite with higher resolution. Moreover, it should also be noted that widely accepted U-corrected Pb-Pb age for CAIs of 4567.30 ± 0.16 Ma is an average of a very few internal CAIs measurements (Amelin et al., 2010; Connelly et al., 2012) which could also be a reason for this discrepancy.

In addition to the canonical abundance of the radiogenic nuclide $[(^{26}Al/^{27}Al)_0$, $(^{182}Hf/^{180}Hf)_0$, $(^{53}Mn/^{55}Mn_0)]$ which is required to determine isochron ages using short-lived chronometers, model age determinations assume homogeneous distribution of the radionuclides and require further estimates for the abundance of the radiogenic nuclide (^{26}Mg/^{24}Mg, ^{182}W/^{184}W, ^{53}Cr/^{52}Cr) and the parent/daughter elemental ratio (Al/Mg, Hf/W, Mn/Cr) in the assumed source reservoir. In the following compilation, if required, the ^{26}Al-^{26}Mg model ages are recalculated using a canonical ^{26}Mg/^{24}Mg abundance of $\delta^{26}Mg_0 = -0.034$ ‰ and parent/daughter elemental ratio in the chondritic reservoir of ^{27}Al/^{24}Mg = 0.101 (Jacobsen et al., 2008). The canonical ^{26}Mg/^{24}Mg abundance is the y-intercept of the bulk CAIs external isochron determined by Jacobsen et al. (2008). Similarly, the ^{182}Hf-^{182}W ages are recalculated using $\varepsilon^{182}W_{chondrites} = (-1.91 \pm 0.08)$, which is the composition of carbonaceous chondrites (Kleine et al., 2004) and a canonical ^{182}W/^{184}W abundance of $\varepsilon^{182}W_0 = -3.49$ which is the y-intercept of the external isochron obtained using CAIs from the Allende, NWA 6870 and NWA 6717 CV3 chondrites (Kruijer et al., 2014a). In case of the ^{53}Mn-^{53}Cr system, the model ages are recalculated using a canonical ^{53}Cr/^{52}Cr abundance of $\varepsilon^{53}Cr_0 = -0.30$ determined in Anand et al. (2021b) by calibrating the ^{53}Mn-^{53}Cr core formation ages with the previously determined ^{182}Hf-^{182}W ages (Kruijer et al., 2017) of magmatic iron meteorite groups.

2.2. Chronology of CAIs

The highest initial $(^{26}Al/^{27}Al)_0$ ratios among all the solar system materials are recorded in CAIs. Jacobsen et al. (2008) and Larsen et al. (2011) produced external isochrons using different bulk CAIs and determined analytically indistinguishable initial $(^{26}Al/^{27}Al)_0$ ratios of $(5.23 \pm 0.15) \times 10^{-5}$ and $(5.25 \pm 0.02) \times 10^{-5}$, respectively. These external isochrons are interpreted to represent the time at which the CAIs or their precursors were isolated from the bulk solar nebula. Internal ^{26}Al-^{26}Mg isochron data for individual CAIs are more complex (e.g., Wasserburg et al., 2012; Makide et al., 2013; Mishra and Chaussidon, 2014; Kööp et al., 2016b; Ushikubo et al., 2017; Krot, 2019; M.C. Liu et al., 2019; Simon et al., 2019; Kawasaki et al., 2018, 2019, 2020; Han et al., 2020; Wada et al., 2020; MacPherson et al., 2010, 2012, 2017a, 2018, 2020, 2022; Dunham et al., 2022; Mane et al., 2022; Fig. 1). Many of these internal CAI isochrons yield initial $(^{26}Al/^{27}Al)_0 \sim 5 \times 10^{-5}$, in agreement with that of the bulk CAIs external isochron or the "canonical" ratio, while several others show a range of initial $(^{26}Al/^{27}Al)_0$ ratios from near 0 to $\sim 5.2 \times 10^{-5}$ which most likely represent (1) disturbances due to reheating events (2) reprocessing in the nebula (3) formation before ^{26}Al was fully mixed into the solar nebula or (4) secondary processing on the meteorite parent. The abundance of CAIs having the canonical $(^{26}Al/^{27}Al)_0$ is consistent with the idea of a very short initial CAI formation interval (M.C. Liu et al., 2019), possibly <20,000 years, while reprocessing of CAIs continued long after primary CAI formation (~condensation) had ceased (Fig. 1).

Apart from the normal CAIs, another group of rare inclusions have been identified that give initial $(^{26}Al/^{27}Al)_0$ ratios much lower than $\sim 5 \times 10^{-5}$, have larger isotopic anomalies in many elements and can be highly mass fractionated. These inclusions are known as FUN inclusions (fractionation and unidentified nuclear effects, highly fractionated but lack large nucleosynthetic anomalies) and PLACs (platy hibonite crystals, lack mass-dependent effects but have larger anomalies than regular CAIs from CV chondrites) (e.g., Park et al., 2017; Kööp et al., 2016a; Fig. 1). Although there is no consensus on how these unusual inclusions formed, current thinking is that they formed from an older dust reservoir in the earliest history of the solar system before ^{26}Al was injected/introduced (e.g., Larsen et al., 2020).

The ^{182}Hf-^{182}W systematics has also been used to obtain isochrons using different bulk CAIs. Kruijer et al. (2014a) obtained an initial $(^{182}Hf/^{180}Hf)_0$ ratio of $(1.018 \times 0.043) \pm 10^{-4}$ that, when anchored to D'Orbigny angrites, gives an age of 4567.9 ± 0.7 Ma. This age agrees within analytical uncertainties with the currently accepted U-corrected Pb-Pb age for CAIs of 4567.30 ± 0.16 Ma (Amelin et al., 2010; Connelly et al., 2012). This agreement supports the homogeneous distribution of short- and long-lived nuclides at the time of CAI formation in the early solar system. This age is taken as "t_0" or the "start of the solar system", although PLACs and FUN inclusions as well as "stardust" (i.e., refractory mineral grains with highly variable isotope compositions (e.g., Hoppe and Zinner, 2000)) could be older (Heck et al., 2020).

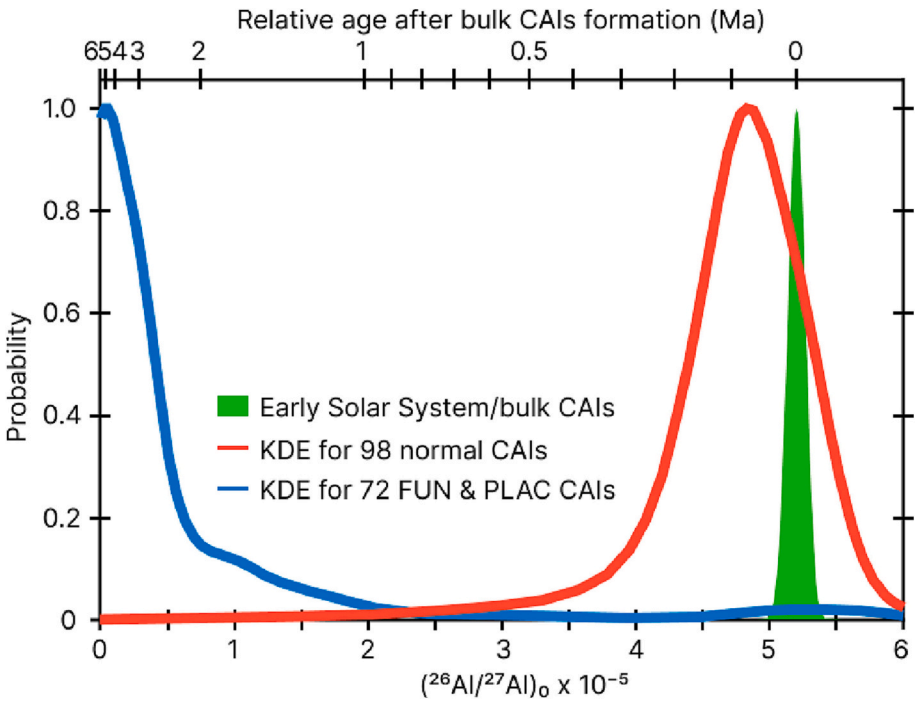

Fig. 1. Kernel Density Estimate (KDE) of initial $(^{26}Al/^{27}Al)_0$ in normal and FUN & PLAC CAIs relative to the canonical/bulk CAIs $(^{26}Al/^{27}Al)_0$ ratio. Ref. Dunham et al. (2022); Wasserburg et al. (2012); Larsen et al. (2020); Ireland (1988); Liu et al. (2009); Park et al. (2017); Kööp et al. (2016b, 2018); MacPherson et al. (2010, 2012, 2018, 2022); Kita et al. (2012); Makide et al. (2013); Mishra and Chaussidon (2014); Kawasaki et al. (2015, 2019, 2020); Krot (2019); Liu et al. (2009); M.C. Liu et al. (2019); Simon et al. (2019); Han et al. (2020); Wada et al. (2020); Fahey et al. (1987); Ireland and Compston (1987); Ireland (1990); Ireland et al. (1992); Sahijpal et al. (2000); Williams et al. (2017); Bodénan et al. (2020a).
Figure modified after Davis (2022).

2.3. Chronology of chondrule formation

2.3.1. Internal isochrons for chondrules: chondrule formation and subsequent reprocessing

All chemically primitive meteorites are chondrites and all of them with the exception of CI chondrites contain visible chondrules. Thus, chondrule formation is an important process the occurred after the first solids were formed and before the accretion of the chondrite parent bodies. Chondrules represent former melt droplets, thus they bear information on a high-temperature process. The ^{26}Al-^{26}Mg system is the most useful chronometer to study the formation and subsequent reprocessing of chondrules because these processes can fractionate Al from Mg to a large extent. The half-life (7.05×10^5 a; Nishiizumi, 2004) of this system is short enough to resolve the chondrule formation ages (Hutcheon and Hutchison, 1989; Hutcheon and Jones, 1995; Kita et al., 2000; Villeneuve et al., 2009; Kita and Ushikubo, 2012; Pape et al.,

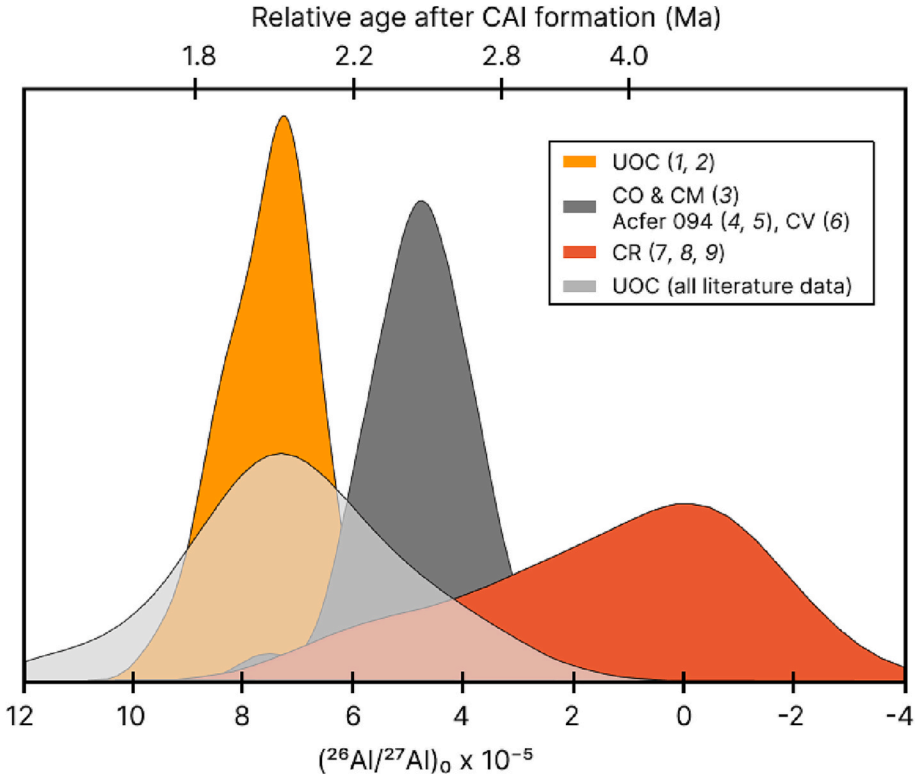

Fig. 2. Compilation of initial $(^{26}Al/^{27}Al)_0$ and corresponding chondrule formation ages (anchored to CAIs using the canonical $(^{26}Al/^{27}Al)_0 = 5.23 \times 10^{-5}$ [Jacobsen et al., 2008; Larsen et al., 2011]) from the least altered chondrites (petrologic subtype 2.9–3.1). References for data: (1–2) Siron et al. (2021, 2022), (3) Fukuda et al. (2022), (4) Ushikubo et al. (2013), (5) Hertwig et al. (2019), (6) Nagashima et al. (2017), (7) Nagashima et al. (2014), (8) Schrader et al. (2017); (9) Tenner et al. (2019). UOC chondrules (L/LL $\leq$ 3.1): Siron et al. (2021, 2022), Hutcheon and Hutchison (1989), Kita et al. (2000), Rudraswami and Goswami (2007), Rudraswami et al. (2008), Villeneuve et al. (2009), Mishra et al. (2010), Pape et al. (2019), Bollard et al. (2019). Figure modified after Fukuda et al. (2022).

2019; Siron et al., 2021, 2022; Fukuda et al., 2022) but long enough to have survived until the accretion of chondrules to form chondrites (Sugiura and Fujiya, 2014).

Pape et al. (2019) presented ^{26}Al-^{26}Mg crystallization ages for a large number of individual ferromagnesian chondrules (glass bearing) from unequilibrated ordinary chondrites of petrologic type <3.15. The initial $(^{26}Al/^{27}Al)_0$ ratios correspond to ^{26}Al-^{26}Mg ages from $1.76^{+0.36}_{-0.27}$ Ma to $2.92^{+0.51}_{-0.34}$ Ma after CAIs using the canonical $(^{26}Al/^{27}Al)_0 = 5.23 \times 10^{-5}$ (Jacobsen et al., 2008; Larsen et al., 2011). One of the two youngest chondrules with an age of ~2.92 Ma was later interpreted to date the time of partial remelting after primary formation in the protoplanetary disk (Pape et al., 2021). The authors combined their data with the previously published ^{26}Al-^{26}Mg ages of the ferromagnesian chondrules in unequilibrated OCs (Hutcheon and Hutchison, 1989; Kita et al., 2000; Mostefaoui et al., 2002; Kita et al., 2005; Rudraswami and Goswami, 2007; Rudraswami et al., 2008; Villeneuve et al., 2009) and showed two major initial $(^{26}Al/^{27}Al)_0$ clusters corresponding to the age of 2.0 and 2.3 Ma after CAIs. However, in a recent study by Siron et al. (2022) a slightly older chondrule formation duration from 1.8 to 2.2 Ma after CAIs was determined for chondrules from unequilibrated ordinary chondrites irrespective of the mesostasis type (plagioclase-bearing or glass bearing) (Fig. 2). These authors argued that the younger ages determined by Pape et al. (2019) and Villeneuve et al. (2009) might be because the glass in chondrule mesostasis (which was the focus in these two studies) is more prone to alteration during secondary processes than plagioclase.

The compilation of chondrule formation ages by Pape et al. (2019) shows a similar range of ages for the ferromagnesian chondrules from L and LL-OCs and CO and CV chondrites (Yurimoto and Wasson, 2002; Kunihiro et al., 2004; Sugiura and Krot, 2007; Kurahashi et al., 2008; Ushikubo et al., 2010; Nagashima et al., 2007, 2008, 2014, 2017; Schrader et al., 2017). Fukuda et al. (2022) updated the ^{26}Al-^{26}Mg chondrule formation duration for CO to ~2.2–2.7 Ma after CAIs and reported first ^{26}Al-^{26}Mg ages for CM chondrules corresponding to ~2.4–2.8 Ma after CAIs. Together with the chondrule formation duration in CV (Nagashima et al., 2017) and OC meteorites (Siron et al., 2021, 2022), the authors inferred a temporal shift in chondrule generation from the inner to the outer part of the protoplanetary disk (Fig. 2). The combined ages for these chondrules supports multiple short-lived episodes of chondrule formation between 1.8 and 3 Ma after CAI formation.

Compared to the other carbonaceous chondrites, ^{26}Al-^{26}Mg chondrule formation ages for CR chondrites are up to 1 Ma younger (Nagashima et al., 2014; Schrader et al., 2017; Tenner et al., 2019). Tenner et al. (2019) reported a mean CR chondrule formation age of 3.8 ± 0.3 Ma after CAIs and suggested that most CR chondrules formed immediately before parent body accretion. Desch et al. (2018) studied the abundances of refractory elements and inclusions in each chondrite group and suggested that the CR chondrule-forming region was outside the CM, CO, and CV chondrule-forming regions. In a recent study, Marrocchi et al. (2022) reported a comprehensive textural and isotopic characterization of type I CR chondrules and concluded that the CR reservoir may have largely belonged to the continuum shown by other carbonaceous chondrites (from matrix-poor CO and CV to matrix rich CI). Similar to the CR chondrites, much younger chondrules have been observed in CB chondrites with ages of 4–5 Ma after CAI formation (e.g., Krot et al., 2005). However, CB chondrules are strongly dominated by metal with minor silicate and thus are inferred to have different genesis than the silicate chondrules in normal chondrites (e.g., Krot et al., 2005; Bollard et al., 2015).

Hellmann et al. (2020) reported internal ^{182}Hf-^{182}W systematics of a macrochondrule from the L5/6 chondrite NWA 819 that corresponds to a model age of 1.4 ± 0.6 Ma after CAIs. These authors also reported ^{182}Hf-^{182}W data for metal from the host chondrite that gives a younger model age of ~11 Ma after CAIs. The internal macrochondrule age was interpreted as the time of metallic melt removal from the chondrule assuming chondritic Hf/W of the reservoir whereas the ^{182}Hf-^{182}W data for metal from the host chondrite gives the time of cooling below the ^{182}Hf-^{182}W closure temperature during thermal metamorphism on the parent body. The difference in the ^{182}Hf-^{182}W model ages between the macrochondrule and the host metal shows that the ^{182}Hf-^{182}W systematics of the bulk macrochondrule were not disturbed during thermal metamorphism.

Ages based on Pb-Pb systematics of single chondrules that are close to CAI formation ages have been reported by Bollard et al. (2017, 2019). These are the only such old ages and were determined with only Pb-Pb system and no short-lived isotope system. The interpretation of these absolute ages relies on the idea that the Pb-Pb system is apparently "assumption free", thus there is no need to know the isotope composition and isotope abundance of the parent and daughter elements to derive an age, only the measurements of Pb isotope ratios are required (e.g. Bollard et al., 2019). Based on the measurements of these old ages Bollard et al. (2019) proposed a late addition of the short-lived isotopes to the early solar system. However, this is difficult to reconcile with the old and reproducible ages of CAIs using different short-lived isotope systems. Thus, the reason for this age difference remains enigmatic. Possible causes for these apparently older Pb-Pb ages could be (a) inheritance of old refractory phases with high U/Pb, (b) heterogeneous U isotope compositions (Reger et al., 2023) and/or (c) loss of intermediate daughters (Pape et al., 2019).

2.3.2. Bulk chondrule ages

Luu et al. (2015) measured the bulk δ^{26}Mg of 14 chondrules from CV3 chondrite Allende and determined a bulk chondrule isochron with an initial $(^{26}Al/^{27}Al)_0$ ratio that corresponds to an age of 1.53 ± 0.18 Ma after CAIs. The isochron is interpreted to date the time when the bulk ^{27}Al/^{24}Mg ratio of the chondrule precursors was established (e.g., during their formation by condensation from the gas). The authors combined their data with the previously published bulk δ^{26}Mg data for Allende and Semarkona (LL3) chondrites (Galy et al., 2000; Bizzarro et al., 2004; Villeneuve et al., 2009) and found that some chondrules plot in between the bulk CAI isochron and the bulk chondrule isochron. The authors suggested that these chondrules represent either the formation of chondrule precursors starting contemporaneously with the formation of CAI precursors and ending ~1.5 Ma later or that all chondrule precursors formed at the same time as CAI precursors (or very close to CAI precursors) and were later reset during the chondrule forming events.

The ^{53}Mn-^{53}Cr system has been used to produce bulk chondrule isochrons for LL, CB, CO and EH chondrites (Yin et al., 2007; Yamashita et al., 2010; Zhu et al., 2019a, 2020a). Zhu et al. (2020a) reported Cr isotope data of nine chondrules in one of the least thermally metamorphosed EH chondrites, Sahara 97,096. Two of these chondrules show mass-independent ^{54}Cr isotope compositions, atypical of enstatite chondrites and similar to carbonaceous chondrites. The authors suggested the transport and mixing of CC-like chondrules into the EC accretion region and only used the EC-like chondrules to produce a bulk chondrule isochron. One more chondrule with a high Fe/Cr ratio was removed from the bulk isochron speculating disturbance due to mild metamorphism and a high abundance of sulfides in the chondrule, as revealed by element mapping. The other six chondrules produced a bulk isochron yielding an initial $(^{53}Mn/^{55}Mn)_0$ ratio which corresponds to an age of 1.60 ± 0.59 Ma after CAIs. The authors interpreted this age as indicating the formation of EC chondrule precursors. In an earlier study, Zhu et al. (2019a) presented bulk chondrule isochron for the CO3 chondrite Ornans. The slope of the isochron corresponds to age within the error of the formation of CAIs. The authors also reported heterogeneity of ε^{54}Cr in CO chondrules suggesting mixing between ε^{54}Cr-depleted and ε^{54}Cr-enriched reservoirs forming in the inner and outer solar system. Owing to the heterogeneously distributed chondrule precursor material for CO chondrules, any chronological interpretation of

the bulk chondrule isochron lacks certainty. Yamashita et al. (2010) reported high-precision Cr isotope ratios for chondrules, and metal grain separated from CB chondrite Gujba. The identical ε^{54}Cr composition of the investigated chondrules and metal grains implies that the Cr isotope systematics of the meteorite was once completely equilibrated. A bulk chondrule and metal grain isochron was produced with a slope corresponding to an age of 4.03 ± 0.81 Ma after CAIs. The authors interpreted this age as the minimum age of chondrule formation. In an earlier study, Yin et al. (2007) presented a bulk chondrule isochron for chondrules extracted from an ordinary chondrite Chainpur (LL3.4) to evaluate the consistency of ^{53}Mn-^{53}Cr, ^{26}Al-^{26}Mg and ^{207}Pb-^{206}Pb chronometers. The slope of the bulk chondrule isochron corresponds to an age of 1.51 ± 1.46 Ma after CAIs and has been inferred as the age of chondrule formation. However, no Fe/Cr and ε^{54}Cr data was provided in the study that can confirm negligible spallogenic Cr contribution and co-genesis of all the chondrules which is required to support the chronological significance of the isochron.

2.3.3. Chondrule components and bulk chondrules-matrix isochrons

High-precision W isotope measurements on chondrules and matrix separated from Allende CV3 chondrite show that both components exhibit complementary ε^{183}W anomalies (Budde et al., 2016b). A ^{182}Hf-^{182}W isochron from three matrices and six chondrule separates corresponds to an age of 2.20 ± 0.57 Ma after CAIs and this age is inferred as the time at which most Allende chondrules formed. To preserve the inner solar system ε^{183}W of bulk chondrites, it is required that chondrules and matrix accreted rapidly to form the chondrite parent body. Rapid accretion of chondrite parent bodies has also been deduced based on the homogeneous composition of the Allende matrix (Neuland et al., 2021). In a separate study, Budde et al. (2018) used the metal, silicate and chondrule separates from four CR chondrites and obtained an isochron. The slope of this isochron corresponds to an age of 3.62 ± 0.28 Ma after CAIs and was inferred as the time of metal-silicate fractionation in CR chondrites. The authors also reported distinct nucleosynthetic W and Mo isotope anomalies in the metal and silicate components of CR chondrites, consistent with the model that the major components of a given chondrite formed together from a single reservoir. However, Sanders and Scott (2022) have recently questioned this interpretation and developed a model suggesting hydrothermal metamorphism can cause complementary isotopic compositions of chondrules and matrix in Allende. These authors showed that anomalous Mo and W, both depleted in s-process isotopes, can easily be leached from their carriers in the matrix, then transported in solution and precipitated preferentially in water-deficient components, such as chondrules, where the aqueous solvent is consumed. Since hydrothermal metamorphism is a planetary process that occurred after accretion, it does not inform about the chondrule-forming mechanisms. If this interpretation is correct, the age of 3.62 ± 0.28 Ma for CR provides information on equilibration on the parent body, but is still a minimum age for the accretion of the planetesimal.

2.4. Chronology of chondrites

2.4.1. Internal isochrons from chondrite components: onset and prograde metamorphism

The ^{53}Mn-^{53}Cr and ^{182}Hf-^{182}W are the two main short-lived chronometers employed to study thermal/aqueous alteration in chondrites. The internal isochrons produced using mineral fractions or chondrite components date the formation of new mineral phases on chondrite parent bodies formed by thermal overprint or aqueous alteration after accretion. Hence, the thermal/aqueous alteration ages constrain the upper limit on the timing of the chondrite parent-body accretion. The ^{26}Al-^{26}Mg system cannot be used to study these parent body processes since the system was practically extinct by the time of the accretion of the parent bodies.

Several studies have focussed on the thermal history of the ordinary chondrite parent bodies and proposed an 'onion-shell' model that predicts that higher temperatures are achieved at greater depths and slightly different times during the evolution of the chondrite parent bodies (e.g., Pellas and Storzer, 1981; Trieloff et al., 2003). This group of meteorites includes material from petrological type 3 (unequilibrated, low thermal overprint) to types 4–6 (equilibrated, higher metamorphic grades) (Van Schmus and Wood, 1967). Since type 3 samples represent the last aggregating material on the chondrite parent bodies, the ^{53}Mn-^{53}Cr and ^{182}Hf-^{182}W thermal/aqueous alteration ages from type 3 chondrites cannot be older than the youngest ^{26}Al-^{26}Mg chondrule formation ages which record the chondrule melting and remelting events that must have occurred before their incorporation into the chondrite parent body. Hence the youngest chondrule formation ages constrain the lower limit on the timing of the chondrite parent-body accretion.

Using the ^{53}Mn-^{53}Cr isotope systematics in ordinary chondrites, Anand et al. (2021a) investigated eight ordinary chondrites from petrological type 3 to 6 and produced two-point isochron ages using chromite and silicate-metal-sulfide fractions. Combined with the ^{53}Mn-^{53}Cr isochron ages for two more samples, Finney (L5, Lugmair and Shukolyukov, 1998) and Ste. Marguerite (H4, Trinquier et al., 2008), thermal metamorphism on the ordinary chondrite parent bodies started at ~2.8 Ma after CAIs and continued up to ~17 Ma after CAIs (Table 2) when the retrograding metamorphic temperatures dropped below the closure temperature of the ^{53}Mn-^{53}Cr system in the core of the planetesimals. Trinquier et al. (2008) and Göpel et al. (2015) studied several carbonaceous chondrites (CI, CV, CO, CM, Tafassasset) and produced ε^{54}Cr vs. ^{55}Mn/^{52}Cr correlation lines for acid leachates from each chondrite. The authors interpreted the correlation lines as isochrons reflecting the time of Cr isotopic equilibration among matrix minerals. However, Zhu et al. (2021a) argued that the correlation lines from carbonaceous chondrite leachates most likely represent mixing lines since chondritic components, e.g., CAIs, chondrules, matrix, metal, and carbonates have different origins and times of formation. Hence any chronological interpretation of these correlation lines lacks certainty.

The cooling history of the H-chondrite parent body was studied by Trieloff et al. (2003) using Pb-Pb, Ar-Ar and Pu fission track ages which are chronometers with different closure temperatures. From the results, they derived an onion-shell model for the parent body with an accretion age prior to ~4 Ma after CAI formation.

Shukolyukov and Lugmair (2004) studied the ^{53}Mn-^{53}Cr isotope systematics in enstatite chondrites by a differential dissolution procedure and produced isochron ages corresponding to 4.71 ± 0.19 Ma after CAIs for Indarch (EH4), 4.34 ± 0.67 Ma for Abbe (EH4) and 9.19 ± 0.26 Ma for Khairpur (EL6) (Table 2). Later studies such as Guan et al. (2007) and Hopp et al. (2021), however, found that the ^{53}Mn-^{53}Cr systematics of enstatite chondrites are easily affected by a variety of processes such as thermal disturbances, diffusion and weathering. Thus, the age constraints for enstatite chondrite accretion and thermal evolution are less certain than for ordinary chondrites, but appear to be very similar.

The chronology and thermal history of the parent bodies of type 4–6H, L and LL ordinary chondrites were studied by Hellmann et al. (2019) using ^{182}Hf-^{182}W systematics. The ^{182}Hf-^{182}W chronometer yielded ages of 3–4 Ma for type 4, 6–14 Ma for type 5, and 9–12 Ma for type 6 chondrites. In type 5 and 6 samples these ages constrain the timing of cooling from peak metamorphic temperatures below the ^{182}Hf-^{182}W closure temperature (Table 2) in the respective sample.

Some carbonaceous chondrites show evidence of hydrous alteration, with the CI chondrites having completely reacted to hydrous mineral assemblages. The ^{53}Mn-^{53}Cr chronometer has also been applied to date this fluid-mediated metamorphism that led to the formation of carbonates (mostly calcite and dolomite) in chondrites (e.g., Endress et al., 1996; Hoppe et al., 2007; deLeuw et al., 2009; Petitat et al., 2011; Fujiya et al., 2012, 2013; Jilly et al., 2014; Jilly-Rehak et al., 2017; Visser et al., 2020). A compilation of ^{53}Mn-^{53}Cr formation ages of carbonates in CI, CR, Tagish Lake (C2) and CM carbonaceous chondrites and C1 and CM-like clasts from complex breccias constrains the timing and extent of

Table 2
^{53}Mn-^{53}Cr and ^{182}Hf-^{182}W chronological data for thermal metamorphism on the parent bodies of ordinary and enstatite chondrites.

Sample	Group	Type	$(^{53}Mn/^{55}Mn)_0$	2σ	Age (Ma)	2σ	Ref.
^{53}Mn-^{53}Cr chronology							
SaU 246	H	3/4	2.35E−06	4.3E−07	5.64	0.90	a
RaS 337	H	3,6	3.03E−06	2.4E−07	4.29	0.41	a
JaH 578	H	6	1.34E−06	1.6E−07	8.64	0.60	a
SaU 228	H	6	9.41E−07	1.48E−07	10.53	0.78	a
JaH 596	L	3	3.96E−06	3.9E−07	2.86	0.50	a
RaS 265	L	3	2.02E−06	2.1E−07	6.45	0.53	a
Dho 1012	L	6	3.80E−07	1.35E−07	15.37	1.62	a
AHu 017	L	6	1.04E−06	2.4E−07	9.99	1.11	a
Finney	L	5	2.70E−07		17.19		b
Ste. Marguerite	H	4	2.78E−06	4.6E−07	4.75	0.82	c
Indarch	EH	4	2.80E−06	1.0E−07	4.71	0.19	d
Abee	EH	4	3.00E−06	4.0E−07	4.34	0.67	d
Khairpur	EL	6	1.21E−06	6E−08	9.19	0.26	d

Sample	Group	Type	$(^{182}Hf/^{180}Hf)_0$	2σ	Age (Ma)	2σ	Ref.
^{182}Hf-^{182}W chronology							
Ste. Marguerite	H	4	7.56E−05	1.3E−06	3.81	0.22	e
ALH 84069	H	5	6.10E−05	1.7E−06	6.57	0.35	e
Zhovtnevyi	H	6	4.86E−05	1.9E−06	9.48	0.49	e
Estacado	H	6	3.84E−05	3.5E−06	12.50	1.12	e
Sarstov	L	4	7.80E−05	2.6E−06	3.41	0.42	e
Tennasilm	L	4	7.56E−05	2.9E−06	3.81	0.48	e
NWA 6630	L	5	6.50E−05	2.8E−06	5.75	0.54	e
Barwell	L	5	5.61E−05	2.0E−06	7.64	0.45	e
Kunashak	L	6	5.16E−05	1.1E−06	8.71	0.27	e
Bruderheim	L	6	4.54E−05	1.9E−06	10.35	0.53	e
NWA 7545	LL	4	7.29E−05	4.2E−06	4.28	0.72	e
Tuxtuac	LL	5	5.47E−05	4.5E−06	7.96	1.01	e
NWA 6629	LL	5	4.57E−05	2.8E−06	10.27	0.76	e
NWA 6935	LL	5	3.75E−05	1.6E−06	12.80	0.54	e
NWA 5755	LL	6	4.41E−05	2.9E−06	10.73	0.82	e
NWA 8192	L	5/6	4.28E−05	7.4E−06	11.11	2.04	f

Ref: (a) Anand et al. (2021a) (b) Lugmair and Shukolyukov (1998) (c) Trinquier et al. (2008) (d) Shukolyukov and Lugmair (2004) (e) Hellmann et al. (2019) (f) Hellmann et al. (2020).

hydrothermal alteration on their parent bodies from ~2 Ma to ~6 Ma after the formation of CAIs (Visser et al., 2020, Table 3, Fig. 3). Bischoff et al. (2021) determined the ^{53}Mn-^{53}Cr systematics in carbonates from the Flensburg (C1-ung) chondrite and derived an age of 2.18 ± 1.15 Ma after CAIs, representing one of the oldest carbonates measured in any chondrite.

Besides chondrites, samples returned from the CI-like asteroid Ryugu were studied recently to obtain ages for dolomite and magnetite precipitation during aqueous alteration using ^{53}Mn-^{53}Cr systematics (Yokoyama et al., 2022; Nakamura et al., 2022; McCain et al., 2023). Yokoyama et al. (2022) reported that dolomite precipitation in the Ryugu samples occurred at $5.21^{+0.79}_{-0.69}$ Ma after CAIs. However, McCain et al. (2023) reported that carbonates in Ryugu formed much earlier - within 1 ± 0.8 Ma after CAI formation. McCain et al. (2023) argued that this difference arises from their use of matrix-matched standards, as opposed to calcite standards used exclusively in previous studies.

In addition to carbonates, the formation of secondary fayalite and kirschsteinite ($CaFeSiO_4$) has been dated using ^{53}Mn-^{53}Cr chronometer to constrain the time scales and hydrothermal evolutionary processes on the CO, CV and ordinary chondrite parent bodies (Hutcheon et al., 1998; Hua et al., 2005; Doyle et al., 2015; Jogo et al., 2009, 2017; MacPherson et al., 2017b). However, Doyle et al. (2015) showed that prior to their study, the ^{53}Mn-^{53}Cr systematics of fayalite were analyzed using inappropriate standards and hence yielded unreliable ages. Doyle et al. (2015) reported ^{53}Mn-^{53}Cr ages of fayalite formed during aqueous alteration in the L3 chondrite Elephant Moraine 90161 at $2.36^{+1.77}_{-1.33}$ Ma, in CV3 chondrite Asuka 881317 at $4.22^{+0.83}_{-0.71}$ Ma and in the CO3-like chondrite MacAlpine Hills 88107 at $5.15^{+0.45}_{-0.42}$ Ma after CAIs (Table 3, Fig. 3). The ^{53}Mn-^{53}Cr chronology of kirschsteinite in the reduced CV3 chondrites Vigarano and Efremovka corresponds to an age of $3.21^{+0.77}_{-0.67}$ Ma after CAIs (MacPherson et al., 2017b, Table 3, Fig. 3). Based on the formation ages of secondary carbonates in hydrated carbonaceous chondrites, and fayalite and kirschsteinite in the CO, CV and ordinary chondrites, it has been inferred that the onset and duration of parent body alteration are similar across all the carbonaceous chondrite groups measured to date (CO, CI, CV, CM, CR and Tagish Lake), but occurred later than metamorphism on the parent bodies of ordinary chondrites (Visser et al., 2020; Suttle et al., 2021).

2.4.2. *Bulk chondrites isochrons: age significance?*

A number of studies in the literature have evaluated the Mn/Cr data for bulk chondrites in a ^{55}Mn/^{52}Cr vs. ε^{53}Cr diagram (Shukolyukov and Lugmair, 2006; Qin et al., 2010a; Trinquier et al., 2008; Göpel et al., 2015; Zhu et al., 2021a, Table 4). However, whether the correlation between chondrites in ^{55}Mn/^{52}Cr vs. ε^{53}Cr space can be interpreted as an isochron is debated (e.g., Scott and Sanders, 2009; Zhu et al., 2021a). Shukolyukov and Lugmair (2006) reported that if the ^{55}Mn/^{52}Cr vs. ε^{53}Cr correlation line for bulk carbonaceous chondrites is considered to be an isochron, it yields information on the Mn and Cr abundances at the time of volatility-driven Mn/Cr fractionation among chondrites or their source reservoir. Trinquier et al. (2008) included Earth, Mars and Vesta on the ^{55}Mn/^{52}Cr vs. ε^{53}Cr diagram for bulk chondrites (OC, EC, CI, CV, and CO) and inferred that the slope of the correlation line corresponds to the time of last isotopic equilibration of Mn and Cr in the protoplanetary disk. Göpel et al. (2015) used the slope of the ^{53}Mn-^{53}Cr evolution diagram for bulk carbonaceous chondrites to determine the solar system initial $(^{53}Mn/^{55}Mn)_0$ and $\varepsilon^{53}Cr_0$ which corresponds to CAI formation. The argument against any chronological significance of a bulk chondrite correlation line is that chondrites as well as chondrite components, such

Table 3
^{53}Mn-^{53}Cr chronological data for aqueous metamorphism on the parent bodies of carbonaceous and ordinary chondrites.

Sample	Mineralogy	Class/group	Type	$(^{53}Mn/^{55}Mn)_0$	2σ	Age (Ma)	2σ	Ref.
Carbonates								
Orgueil	Dolomite	CI		3.24E−06	4.4E−07	3.93	0.69	a
Orgueil	Dolomite	CI		3.13E−06	8.4E−07	4.11	1.27	e
Y 980115	Dolomite	CI		3.37E−06	8.2E−07	3.72	1.16	a
Ivuna	Dolomite	CI		2.78E−06	5.1E−07	4.75	0.90	e
Ivuna	Dolomite	CI		2.64E−06	3.9E−07	5.02	0.74	a
Alais	Dolomite	CI		3.68E−06	6.4E−07	3.25	0.86	e
Kaidun	Carbonate	CI-clast		4.20E−06	4.0E−07	2.54	0.49	f
Kaidun	Carbonate	CI-clast		2.89E−06	4.1E−07	4.54	0.71	e
Ryugu	Dolomite	CI		2.55E−06	3.5E−07	5.21	0.69	g
Ryugu	Dolomite	CI		6.10E−06	0.90E−06	1.00	0.80	h
Murchison	Calcite	CM	2.5	2.66E−06	7.9E−07	4.98	1.39	c
Y 791198	Calcite	CM	2.4	3.40E−06	7.4E−07	3.67	1.05	c
ALH 83100	Dolomite	CM	2.1	2.79E−06	4.7E−07	4.73	0.83	c
Sayama	Dolomite	CM	2.1	3.38E−06	4.0E−07	3.70	0.60	c
Sutter's Mill	Dolomite	CM	2.0/2.1	3.42E−06	3.6E−07	3.64	0.53	b
Kaidun-1	Carbonate	CM-clast		4.66E−06	1.20E−06	1.99	1.22	e
Renazzo	Dark dolomites	CR	2.4	3.70E−06	1.70E−06	3.22	2.02	d
Tagish Lake	Dolomite	C-ung	2	3.16E−06	6.9E−07	4.06	1.05	a
Flensburg	Carbonate	C-ung	1	4.50E−06	1.08E−06	2.18	1.15	i
Silicates								
Vigarano + Efremovka	Kirschsteinite	CV	3	3.71E−06	5.0E−07	3.21	0.67	j
Asuka 881317	Fayalite	CV	3	3.07E−06	4.4E−07	4.22	0.71	k
MAC 88107	Fayalite	CO	3.0–3.1	2.58E−06	2.1E−07	5.15	0.42	k
EET 90161	Fayalite	L	3.05	4.35E−06	1.23E−06	2.36	1.33	k

Ref: (a) Fujiya et al. (2013) (b) Jilly et al. (2014) (c) Fujiya et al. (2012) (d) Jilly-Rehak et al. (2017) (e) Visser et al. (2020) (f) Petitat et al. (2011) (g) Yokoyama et al. (2022) (h) McCain et al. (2023) (i) Bischoff et al. (2021) (j) MacPherson et al. (2017b) (k) Doyle et al. (2015).

as chondrules, matrix, metals, CAIs and AOAs, all formed at different times and may have different source regions. Zhu et al. (2021a) reported comprehensive Mn/Cr bulk chondrite data and assessed the $^{55}Mn/^{52}Cr$ vs. $\varepsilon^{53}Cr$ correlation lines for carbonaceous, enstatite, ordinary and Rumuruti chondrites, individually and combined, and interpreted the $^{55}Mn/^{52}Cr$ vs. $\varepsilon^{53}Cr$ correlation line as the result of multiple end-member mixing of different chondritic components (Table 4, Fig. 4).

Similar to the ^{53}Mn-^{53}Cr systematics, bulk chondrites have also been found to correlate on a $^{26}Mg/^{24}Mg$ vs. $^{27}Al/^{24}Mg$ isochron diagram ($^{26}Mg/^{24}Mg$ expressed as $\Delta'^{26}Mg$) and interpreted to have a common, canonical $(^{26}Al/^{27}Al)_0$ in their parent bodies (Schiller et al., 2010b; Kita et al., 2013). In a recent study, Luu et al. (2019) showed that with the exception of CR and EC, bulk chondrites including CV, CI, CM, CO, CK, H and LL, define a primordial ^{26}Al-^{26}Mg isochron (Fig. 5). The marked departure of CR and EC from this array is interpreted as due to slightly higher $\Delta'^{26}Mg$ of EC as result of their relatively late condensation and loss of refractory phases and, anomalously low $(\Delta'^{26}Mg)_0$ of CR related to their markedly elevated $\delta^{15}N$. Nevertheless, the slope of this isochron yields an initial $(^{26}Al/^{27}Al)_0 = 4.7 \pm 0.8 \times 10^{-5}$, which is within the uncertainty of the canonical $(^{26}Al/^{27}Al)_0$ ratio defined by CAIs (Jacobsen et al., 2008; Larsen et al., 2011) and indicates a near homogeneous initial $(^{26}Al/^{27}Al)_0$ during the formation of CAIs and precursor grains to the different meteorite groups (Luu et al., 2019).

2.5. Chronology of magmatic iron meteorites

The ^{182}Hf-^{182}W and ^{53}Mn-^{53}Cr short-lived chronometers are commonly used to constrain different stages in the evolution of iron meteorite parent bodies (Goldstein et al., 2009). Both systems can examine the timescales and mechanisms of metal segregation in the iron meteorite parent bodies since the parent and daughter elements of both systems have different geochemical behavior resulting in Hf/W and Mn/Cr fractionation during the metal-silicate (-sulfide) separation including core formation (e.g., Kleine et al., 2005; Kruijer et al., 2014b, 2017; Anand et al., 2021b; Spitzer et al., 2021). Additionally, ^{53}Mn-^{53}Cr has also been applied to phosphates in IIIAB iron meteorites to determine cooling ages (Sugiura and Hoshino, 2003).

Kruijer et al. (2017) examined a large set of magmatic iron meteorite groups (IIAB, IID, IIIAB, IVA, IVB, IC, IIC, IIF, IIIE, IIIF) using the ^{182}Hf-^{182}W chronometer and determined core formation ages of ~0.3–1.8 Ma after CAIs for the non-carbonaceous iron meteorite parent bodies and ~2.2–2.8 Ma for the carbonaceous iron meteorite parent bodies (Table 5, Fig. 6). Anand et al. (2021b) used the ^{53}Mn-^{53}Cr chronometer to determine chromite/daubréelite model ages from the three largest magmatic iron meteorite groups, IIAB, IIIAB and IVA. The authors calibrated the ^{53}Mn-^{53}Cr model ages with the ^{182}Hf-^{182}W core formation ages determined by Kruijer et al. (2017) and constrained the solar system initial $\varepsilon^{53}Cr_0$ to -0.30 ± 0.05. Tornabene et al. (2020) updated the ^{182}Hf-^{182}W core formation age of IIC iron meteorites to 3.2 ± 0.5 Ma after CAIs and Tornabene et al. (2023) updated the ^{182}Hf-^{182}W core formation age of IC iron meteorites to 1 ± 0.4 Ma after CAIs. However, in a recent study, Spitzer et al. (2021) identified a small nucleosynthetic Pt isotope anomaly in some ungrouped iron meteorites that has significant implications for the ^{182}Hf-^{182}W chronology of iron meteorites. Due to this nucleosynthetic Pt isotope anomaly, the authors suggested a ~1 Ma upward (younger) revision of the ^{182}Hf-^{182}W ages previously determined by Kruijer et al. (2017) and Tornabene et al. (2020, 2023) (Table 5, Fig. 6). Moreover, ^{182}Hf-^{182}W model ages of iron meteorites strongly depend on the Hf/W ratio and the associated W isotopic composition estimated for their precursors. So far, all studies that have determined ^{182}Hf-^{182}W core formation ages have assumed a carbonaceous chondrites-like Hf/W ratio of all the iron meteorite parent bodies. However, studies such as Lee and Halliday (2000) Hellmann et al. (2019) and Hellmann and Walker (2023), have shown that the parent bodies of enstatite chondrites and ordinary chondrites, that likely originated in the inner solar system, evolved with Hf/W ratios that are distinct from that of the carbonaceous chondrites, which are derived from the outer solar system. Hence, the current ^{182}Hf-^{182}W model ages of non-carbonaceous iron meteorites originating from the inner solar system might be erroneous. Recently, Hellmann and Walker (2023) re-evaluated the ^{182}Hf-^{182}W model ages of non-carbonaceous iron meteorites using the Hf/W ratio of EH chondrites and suggested a shift in the non-carbonaceous iron meteorites core formation ages by up to ~0.7 Ma towards a later formation. As a consequence, the younger core formation

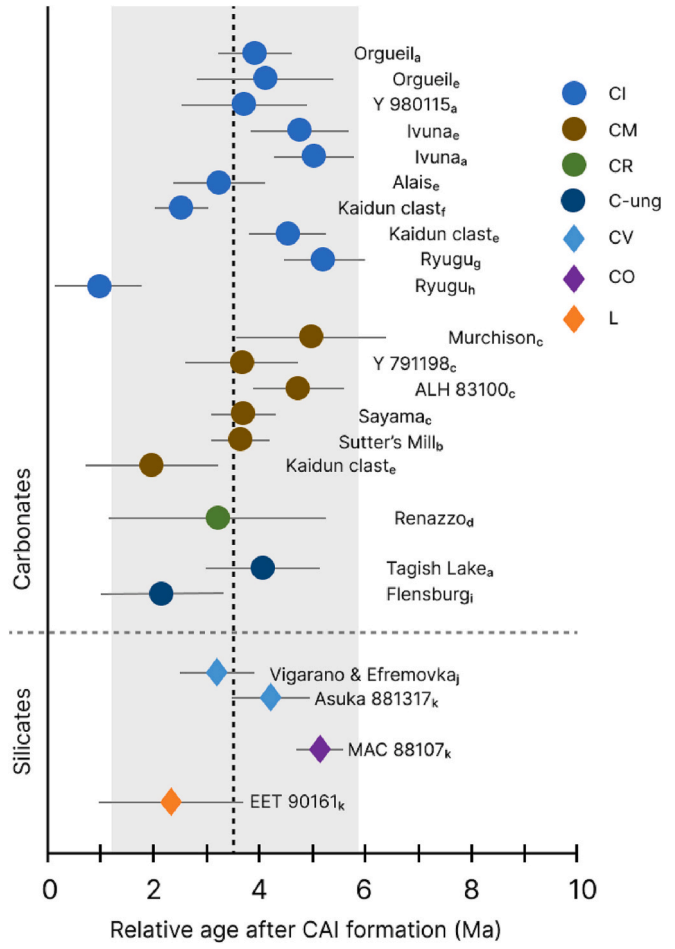

Fig. 3. The timing of aqueous alteration on the parent bodies of carbonaceous and ordinary chondrites inferred from ^{53}Mn-^{53}Cr chronology of the secondary carbonates and silicates. The dotted line and shaded region represent the mean and 2σ of the ages respectively. Ref: (a) Fujiya et al. (2013) (b) Jilly et al. (2014) (c) Fujiya et al. (2012) (d) Jilly-Rehak et al. (2017) (e) Visser et al. (2020) (f) Petitat et al. (2011) (g) Yokoyama et al. (2022) (h) McCain et al. (2023) (i) Bischoff et al. (2021) (j) MacPherson et al. (2017b) (k) Doyle et al. (2015).

ages suggested by (1) Spitzer et al. (2021) due to nucleosynthetic Pt isotope anomaly and (2) Hellmann and Walker (2023) due to distinct Hf/W ratio of the non-carbonaceous reservoir, an even lower solar system initial $\varepsilon^{53}Cr_0$ ($<-0.30 \pm 0.05$) is expected based on combined ^{53}Mn-^{53}Cr and ^{182}Hf-^{182}W model ages of the magmatic iron meteorites.

The combined ages for core formation based on ^{53}Mn-^{53}Cr and ^{182}Hf-^{182}W systematics of magmatic irons constrain a time-interval of 1 to 2 Ma for irons from the non-carbonaceous reservoir, and a slightly later formation age of 2 to 4 Ma after CAIs for irons from the carbonaceous reservoir. Thus, the cores from which the non-carbonaceous iron meteorites originated accreted in a time interval between the accretion of CAIs and the formation of the first chondrules.

Apart from the metal-silicate separation ages of the iron meteorite parent bodies, Sugiura and Hoshino (2003) investigated ^{53}Mn-^{53}Cr systematics in phosphates (sarcopside, graftonite, beusite, galileiite, and johnsomervilleite) in IIIAB iron meteorites and determined ^{53}Mn-^{53}Cr cooling ages that range from 2.60 ± 1.47 Ma to 22.66 ± 0.43 Ma after CAIs.

2.6. Chronology of primitive achondrites: acapulcoite-lodranites, brachinites and winonaites

There are no published chronological data reported for brachinites using short-lived isotope systems. For winonaites, only one high-precision ^{182}Hf-^{182}W study is available by Schulz et al. (2010) who derived an isochron from bulk, silicate and metal fractions from samples HaH 193, Mount Morris, Winona, NWA 4024 and NWA 1457. The intercept of the isochron yields a model age of $6.60^{+3.20}_{-2.56}$ Ma after CAIs, which is inferred as the time of a melting event on the winonaites parent body. In contrast, the slope of the isochron corresponds to an age of $14.94^{+2.99}_{-2.42}$ Ma after CAIs and is interpreted to date the timing of metamorphic redistribution. Schulz et al. (2010) also produced an isochron after combining the bulk, metal and silicate fractions from two acapulcoite samples Dhofar 125 and Monument Draw. The slope of this isochron corresponds to an age of $4.70^{+1.22}_{-1.11}$ Ma after CAIs and is interpreted to date the melting event on the acapulcoite parent body. This age obtained from combined acapulcoite fractions is also in agreement with the previously reported ^{182}Hf-^{182}W combined isochron age of 5.76 ± 0.67 Ma after CAIs determined from acapulcoites NWA 2775 and Dhofar 125, and internal isochron age of 6.28 ± 0.84 Ma determined from lodranite NWA 2627 (Touboul et al., 2009). The isochron ages are interpreted to date the timing of the ^{182}Hf-^{182}W system below the closure temperature (Table 6).

2.7. Chronology of differentiated achondrites: aubrites, angrites, ureilites and HEDs

The ^{26}Al-^{26}Mg studies of aubrites show that the absence of excess ^{26}Mg constrains their formation to >2.9 Ma after CAI formation (e.g., Baker et al., 2012). Shukolyukov and Lugmair (2004) studied the ^{53}Mn-^{53}Cr isotope systematics of aubrites Pena Blanca Spring, Bishopville and Cumberland Falls, through a sequential digestion experiment and showed a lack of internal isochrons in the studied samples due to Mn/Cr redistribution after ^{53}Mn had decayed. However, the whole-rock data for aubrites was used to produce an external isochron that yields an age of 6.51 ± 1.19 Ma after CAIs. Zhu et al. (2021b) added more main group aubrites to the bulk-rock isochron and updated the slope corresponding to an age of 5.21 ± 1.00 Ma after CAIs (Table 7). The authors also used the mass-dependent Cr isotope data and mass-independent ^{54}Cr anomalies to show that the bulk isochron is a mixing line between lithologies with abundant Cr-rich sulfide and lithologies with Cr-poor silicates. Consequently, the age obtained from the isochron was inferred as the time of silicate and sulfide mineral crystallization or the age of silicate differentiation on the parent body of the main-group aubrites.

Angrites are mafic to ultramafic meteorites that formed by melting in the mantle of an early differentiated planetesimal(s). Kleine et al. (2012) investigated a comprehensive suite of angrites and reported ^{182}Hf-^{182}W internal isochrons obtained using mineral separates, whole rocks and fine fractions. The isochrons correspond to ages ranging from 4.54 ± 0.30 to 11.93 ± 0.75 Ma after CAIs and are inferred as the time of crystallization. Similarly, ^{26}Al-^{26}Mg internal isochrons based on mineral separates from angrites Asuka 881394, D'Orbigny, Sah 99555 and NWA 1670 correspond to crystallization ages ranging from 3.91 ± 0.06 to 5.23 ± 0.05 Ma after CAIs (Wadhwa et al., 2009; Schiller et al., 2015). Both internal and external bulk-rock isochrons are published for angrites using ^{53}Mn-^{53}Cr systematics (Table 7). Internal isochrons for angrites, D'Orbigny, Sahara 99555, Asuka 881371, NWA 1670 and LEW 86010 yield crystallization ages from 3.01 ± 0.31 to 9.01 ± 0.29 Ma after CAIs (Lugmair and Shukolyukov, 1998; Glavin et al., 2004; Sugiura et al., 2005; Wadhwa et al., 2009). Zhu et al. (2019b) reported ^{53}Mn-^{53}Cr systematics for seven bulk angrites and produced an external isochron that corresponds to an age of 4.06 ± 0.18 Ma after CAIs. All the angrites

Table 4
A compilation of initial $(^{53}Mn/^{55}Mn)_0$, $\varepsilon^{53}Cr_0$ and corresponding ages inferred from the bulk chondrite $^{55}Mn/^{52}Cr$ vs. $\varepsilon^{53}Cr$ plots.

Samples	$(^{53}Mn/^{55}Mn)_0$	2σ	$\varepsilon^{53}Cr_0$	2σ	Age? (Ma)	2σ	Ref
Bulk CC	8.50E−06	1.50E−06	−0.21	0.09	−1.22	0.87	a
Bulk OC, EC, CI, CV, CO and terrestrial planets	6.53E−06	1.93E−06	−0.23	0.11	0.19	1.38	b
Bulk CC	6.80E−06		−0.18		−0.03	0.00	c
Bulk OC	5.39E−06	2.23E−06	−0.16	0.05	1.21	1.85	d
Bulk OC, EC, CI, CR, CB, CH, CK, CV, CO, CM	3.23E−06	8.9E−07	0.00	0.05	3.95	1.30	d

Ref: (a) Shukolyukov and Lugmair (2006) (b) Trinquier et al. (2008) (c) Göpel et al. (2015) (d) Zhu et al. (2021a).

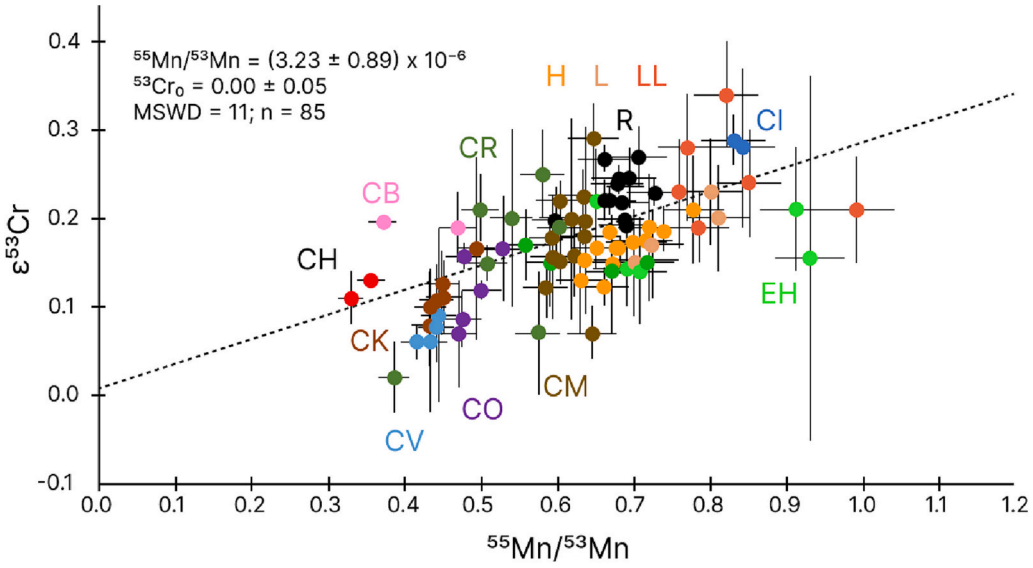

Fig. 4. $\varepsilon^{53}Cr$ vs. $^{55}Mn/^{52}Cr$ diagram for bulk chondrites. See Zhu et al. (2021a) for data and references.
Figure modified after Zhu et al. (2021a) who interpret the best fit ^{53}Mn-^{53}Cr correlation line as a mixing line rather than an isochron.

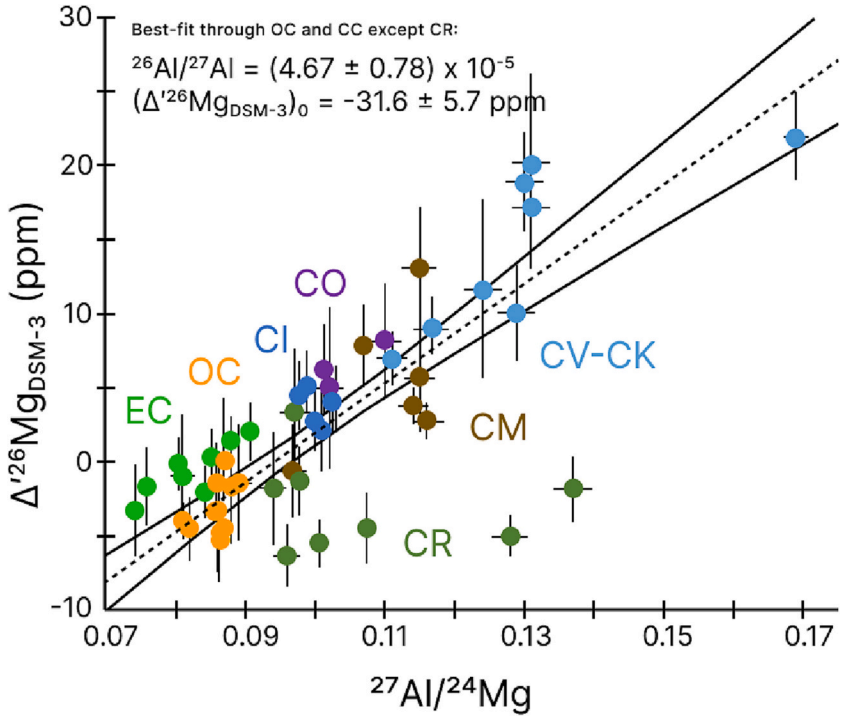

Fig. 5. $\Delta'^{26}Mg_{DSM-3}$ (DSM-3 international terrestrial standard, see Luu et al. (2019) for the definition) vs. $^{27}Al/^{24}Mg$ diagram for bulk chondrites. See Luu et al. (2019) for data and references.
Figure modified after Luu et al. (2019).

Table 5
A compilation of group averaged initial $\varepsilon^{182}W_0$ compositions of magmatic iron meteorites and corresponding ^{182}Hf-^{182}W model ages for core formation.

Group	Corrected to $\varepsilon^{196}Pt = 0$		Ref.	Recalculated*			
	$\varepsilon^{182}W$ pre-exposure (6/4)	2σ		Corrected to $\varepsilon^{196}Pt = -0.06 \pm 0.01$		Δt_{CAI} (6/4) [Ma]	2σ
				$\varepsilon^{182}W$ pre-exposure (6/4)	2σ		
NC							
IC	−3.45	0.04	a	−3.37	0.04	1.0	0.7
IC	−3.37	0.05	b	−3.29	0.05	1.7	0.8
IIAB	−3.40	0.03	a	−3.32	0.03	1.4	0.7
IIIAB	−3.35	0.03	a	−3.27	0.03	1.9	0.7
IIIE	−3.28	0.06	a	−3.20	0.06	2.6	0.9
IVA	−3.32	0.05	a	−3.24	0.05	2.2	0.8
CC							
IIC	−3.20	0.12	a	−3.12	0.12	3.4	1.4
IIC_{Os}	−3.14	0.09	c	−3.14	0.09	3.2	1.1
Wiley	−3.23	0.11	a	−3.15	0.11	3.1	1.3
$Wiley_{Os}$	−3.08	0.13	c	−3.08	0.13	3.9	1.6
IID	−3.23	0.04	a	−3.15	0.04	3.1	0.7
IIF	−3.21	0.05	a	−3.13	0.05	3.3	0.8
IIIF	−3.24	0.10	a	−3.16	0.10	3.0	1.2
IVB	−3.18	0.05	a	−3.10	0.05	3.6	0.8
SBT_{Os}	−3.25	0.08	d	−3.25	0.08	2.1	1.0
Babb's Mill	−3.26	0.13	e	−3.26	0.13	2.1	1.4
ILD 83500	−3.29	0.15	e	−3.29	0.15	1.7	1.5
Guffey	−3.10	0.12	e	−3.10	0.12	3.7	1.4
Hammond	−3.13	0.16	e	−3.13	0.16	3.3	1.8

Ref: (a) Kruijer et al. (2017) (b) Tornabene et al. (2023) (c) Tornabene et al. (2020) (d) Hilton et al. (2019) (e) Spitzer et al. (2021).
* Recalculated pre-exposure $\varepsilon^{182}W$ (6/4) and corresponding ^{182}Hf-^{182}W model ages as per Spitzer et al. (2021).

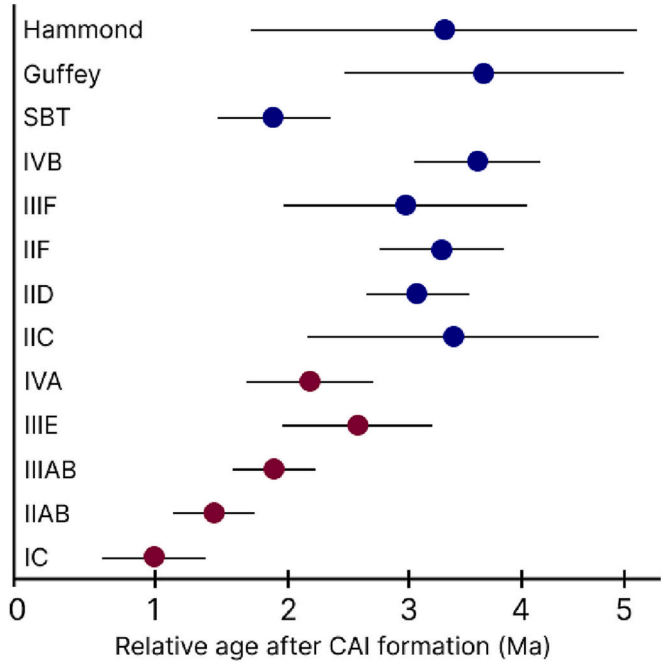

Fig. 6. ^{182}Hf-^{182}W model ages for metal segregation in the parent bodies of magmatic iron meteorites. Pre-exposure $\varepsilon^{182}W$ are compiled in Table 5. Ref. for data: Kruijer et al. (2017); Tornabene et al. (2023); Tornabene et al. (2020); Hilton et al. (2019); Spitzer et al. (2021).
Figure modified after Spitzer et al. (2021).

show homogeneous $\varepsilon^{54}Cr$ values and the age obtained from the bulk-angrite isochron is inferred as the time of Mn/Cr fractionation through magmatic processes and mantle-crust differentiation.

Ureilites are products of partial melting of the mantle in a carbon-rich asteroid (e.g., Goodrich et al., 2004; Warren et al., 2006) and have been extensively studied using the short-lived chronometers ^{182}Hf-^{182}W and ^{53}Mn-^{53}Cr. Earlier studies on ureilites have reported ^{55}Mn-^{52}Cr internal isochrons yielding crystallization ages ranging from 3.75 ± 0.62 to 4.63 ± 0.20 Ma after CAIs (Goodrich et al., 2010; Yamakawa et al., 2010). Budde et al. (2015) presented ^{182}Hf-^{182}W systematics on 12 whole-rock ureilites that give a mean model age of 3.3 ± 0.7 Ma after CAIs and this age is inferred as the time of silicate melt extraction in the ureilite parent body (Table 7). Zhu et al. (2020b) reported a bulk ureilite ^{53}Mn-^{53}Cr isochron that corresponds to an age of 0.62 ± 1.25 Ma after CAIs. The age obtained from this bulk-ureilite isochron is inferred as the time of an early partial melting event on the ureilite parent body. However, the isochron is mostly constrained by a single data point with an unusually high $^{55}Mn/^{52}Cr$ obtained from a ureilitic trachyandesite (ALM-A).

The meteorites belonging to the HEDs clan are widely considered to originate from early magmatic activity on the Vesta parent body. Hublet et al. (2017) used the ^{26}Al-^{26}Mg chronometer to study basaltic and cumulate eucrites, and diogenites. Internal isochrons obtained from mineral separates constrain the crystallization of basaltic eucrites at $2.66^{+1.39}_{-0.58}$ Ma and cumulate eucrites from $5.48^{+1.56}_{-0.60}$ Ma to >7.25 Ma after CAIs. Diogenites, however, show an absence of ^{26}Mg deficits indicating their formation after the complete extinction of ^{26}Al. The ^{182}Hf-^{182}W study of basaltic eucrites yields three internal isochron age groups of ~4 Ma, ~11 Ma and ~22 Ma after CAIs (Touboul et al., 2015) and indicates an extended period of magmatic and metamorphic activity on the HED parent body. Similarly, Roszjar et al. (2016) reported ^{182}Hf-^{182}W chronometry of individual zircon grains from six basaltic eucrites that show distinct growth episodes ranging from 4532^{+6}_{-11} Ma to 4565.0 ± 0.9 Ma indicating that the mantle of 4 Vesta generated basaltic melts for ~35 Ma.

2.8. Chronology of stony iron meteorites: mesosiderites and pallasites

Mesosiderites are stony-iron meteorites, consisting of eucrite-like silicates and Fe-Ni metal. Internal ^{53}Mn-^{53}Cr isochrons obtained from Vaca Muerta mesosiderite clasts (basaltic and orthopyroxenitic) show that Cr isotopes equilibrated after ^{53}Mn was extinct (Wadhwa et al., 2003). Zircon, an accessory phase in mesosiderites has been used for ^{182}Hf-^{182}W chronology to constrain ancient events such as reheating of the mesosiderite parent body (e.g., Ireland, 1991). Koike et al. (2017) conducted in-situ ^{182}Hf-^{182}W dating of zircons from mesosiderite Asuka 882023 and reported an age of 35.0 ± 5.67 Ma after CAIs. This age was interpreted as the timing of zircon formation, which occurred much later than the crustal differentiation of the parent body.

Pallasites are a group of stony-iron meteorites mainly composed of olivine and Fe-Ni metal. Tungsten-Mo and Cr-O isotope studies suggest an impact mix of the silicate and metal portions that stem from distinct isotopic reservoirs (Kruijer et al., 2022; Windmill et al., 2022). The $\varepsilon^{182}W$ of the metal from main group pallasites gives a mean ^{182}Hf-^{182}W model age of 1.7 ± 0.6 Ma after CAIs and is interpreted as the timing of metal-silicate fractionation of the impactor body from which the metal is derived (Kruijer et al., 2022). Windmill et al. (2022) obtained a ^{53}Mn-^{53}Cr isochron for the olivine fractions from the main group pallasites that corresponds to an age of 9.32 ± 0.84 Ma after CAIs. The silicate portion originated from the impacted body and the isochron from the olivine fractions is inferred as the closure of the ^{53}Mn-^{53}Cr decay system. Overall robust age constraints for pallasites are still rare.

Table 6
^{182}Hf-^{182}W chronology of winonaites and acapulcoite-lodranites.

Primitive achondrite	ε^{182}W	2σ	Model age (Ma)	2σ	$(^{182}Hf/^{180}Hf)_0$	2σ	Age (Ma)	2σ	Ref
Winonaite									
External isochron from winonaites HaH 193, Mount Morris, Winona, NWA 4024 & NWA 1457	−2.85	0.21	6.6	3.2	3.18E−05	6.6E−06	14.94	2.42	a
Acapulcoite/lodranite									
External isochron from acapulcoites Dhofar 125 & Monument Draw					7.06E−05	6.4E−06	4.70	1.11	a
External isochron from acapulcoites NWA 2775 & Dhofar 125					6.50E−05	3.5E−06	5.76	0.67	b
Internal Isochron from Lodranite NWA 2627					6.24E−05	4.2E−06	6.28	0.84	b

Ref: (a) Schulz et al. (2010) (b) Touboul et al. (2009).

2.9. Chronology of ungrouped achondrites

A number of ungrouped achondrites have been studied using short-lived chronometers to obtain insight into accretion, melting, and differentiation processes occurring on a diverse group of planetesimals in the early solar system. The ages obtained using ^{26}Al-^{26}Mg, ^{182}Hf-^{182}W and ^{53}Mn-^{53}Cr chronometers are mostly inferred as the time of isotopic closure below the respective closure temperatures. Sanborn et al. (2019) investigated the carbonaceous achondrite NWA 6704/6693 using the ^{26}Al-^{26}Mg and ^{53}Mn-^{53}Cr systems. The ^{26}Al-^{26}Mg isochron obtained using pyroxene and plagioclase mineral separates yielded an age of 5.38 ± 0.12 Ma after CAIs. The ^{53}Mn-^{53}Cr isochron based on chromite, metal, whole-rock and pyroxene fractions corresponds to an age of 5.13 ± 0.66 Ma after CAIs. Bouvier et al. (2011) studied the ^{26}Al-^{26}Mg systematics in carbonaceous achondrite NWA 2976 (thought to be paired with NWA 011 and NWA 2400, Connolly et al., 2007) and obtained an isochron that indicates a time of formation of 5.15 ± 0.04 Ma after CAIs. Similarly, ungrouped achondrites NWA 7325 (non-carbonaceous, Goodrich et al., 2017) and Asuka 881394 (non-carbonaceous, Wimpenny et al., 2019) are dated using ^{26}Al-^{26}Mg systematics and the obtained internal isochrons yield formation ages of 5.42 ± 0.05 Ma after CAIs for NWA 7325 (Koefoed et al., 2016) and 3.75 ± 0.08 Ma for Asuka 881394 (Wimpenny et al., 2019). The carbonaceous achondrite Tafassasset has been dated by ^{182}Hf-^{182}W and ^{53}Mn-^{53}Cr chronometers (Breton et al., 2015; Göpel et al., 2015). The ^{182}Hf-^{182}W isochron obtained using separate mineral fractions yielded an age of 4.10 ± 1.16 Ma after CAIs (Breton et al., 2015). Göpel et al. (2015) investigated ^{53}Mn-^{53}Cr systematics in Tafassasset and defined an isochron using separated mineral fractions and sequentially digestion leachates corresponding to an age of 3.80 ± 0.25 Ma after CAIs. Non-carbonaceous achondrite NWA 5363/NWA 5400 has been studied using the ^{182}Hf-^{182}W systematics and the mean ε^{182}W of the samples equates to a two-stage model age of Hf/W fractionation from a chondritic reservoir of 2.2 ± 0.8 Ma after CAIs (Burkhardt et al., 2017). Recently, Fang et al. (2022) investigated ^{26}Al-^{26}Mg systematics in the andesitic achondrite EC 002 and reported an internal isochron age of 1.87 ± 0.01 Ma after CAIs, which makes EC 002 the oldest volcanic rock dated so far. Anand et al. (2022) used the ^{53}Mn-^{53}Cr systematics in EC 002 and obtained an internal isochron using sequential digestion leachates that correspond to an age of 1.88 ± 0.42 Ma after CAIs. The authors also used the combined ^{54}Cr and Δ^{17}O isotope compositions of EC 002 to confirm its origin in the non-carbonaceous reservoir. Before the ^{26}Al-^{26}Mg and ^{53}Mn-^{53}Cr systematics of EC 002, the status of the oldest felsic igneous rock was held by carbonaceous achondrite NWA 11119 which was dated at 3.61 ± 0.05 Ma after CAIs using the ^{26}Al-^{26}Mg chronometer (Srinivasan et al., 2018).

3. Discussion and conclusions

Fig. 7 summarizes the timing of events and processes in the early solar system from the time of CAI formation (t_0) to the accretion of the first large planetesimals. The samples are separated into the two main groups representing the NC- and CC-reservoirs as suggested by Warren (2011). These reservoirs may correspond to the inner (NC-reservoir) and outer (CC-reservoir) solar system separated early by Jupiter (Kruijer et al., 2017). All these ages define processes and events associated with chemical fractionation that is also expressed in the separation of a radioactive parent from its radiogenic daughter element. Certain processes and events apparently occurred in a very specific time interval; others occurred multiple times or continuously over the first ca. 10 Ma of the solar system. Specific and unique time intervals are observed for CAI formation, formation of silicate chondrules and aqueous alteration on planetary bodies. Accretion, metamorphism, differentiation of planetesimals and planets and disruption of planetary bodies by collisions occurred continuously throughout this early time interval. A comparison of materials from the NC and CC reservoirs (i.e., inner vs. outer solar system) shows a slight indication that the different processes (i.e., first core formation, first chondrule formation) occurred earlier in the NC than the CC reservoir. However, this temporal offset, if real, is <1 Ma.

The oldest precisely dated solids from the solar system are CAIs in chondrites. It is thus justified to use them to define the "beginning of the solar system", t_0. These highly refractory inclusions are most commonly preserved in carbonaceous chondrites and very rarely in non-carbonaceous chondrites. Although their strong depletion in moderately volatile elements indicates high-temperature processing, very likely close to the Sun, they are mostly found in carbonaceous chondrites, which formed at a greater radial distance than non-carbonaceous chondrites and hence required their radial transport to the outer solar system (e.g., Burkhardt et al., 2019). After CAIs the next groups of ages are recorded in magmatic irons, which represent cores of differentiated planets. The oldest of these cores date within <1 Ma of CAI formation (Kruijer et al., 2014b, 2017; Anand et al., 2021b). Core formation in planetesimals started in the inner NC-reservoir slightly earlier than in the outer CC reservoir (Table 5). Generally, melt generation and the efficiency of planetary differentiation decrease with increasing time of accretion relative to CAIs, smaller size of the planetesimal, and decreasing accretion rate of planetary bodies. The later the onset time of accretion the larger planetesimal has to be to enable large scale melting and major chemical differentiation, particularly core formation (Neumann et al., 2012). This is because ^{26}Al was the main heat source only in the early solar system. Impacts and accretion energy were the dominant heat sources only after ^{26}Al was extinct. The oldest iron meteorites that formed contemporaneously, or shortly after CAIs, attest to the melting of their parent bodies due to heating by the decay of the short-lived isotope ^{26}Al. These early core formations occurred on several different planetesimals and are well documented by numerous iron meteorites. It is relevant to note that no material has yet been found that corresponds to the silicate portion of these oldest differentiated bodies. Only rarely can silicates be related to iron meteorites. This correlation is only possible for examples where core formation occurred >2 Ma after t_0. Such pairings are main group pallasites and howardite-eucrite-diogenites with IIIAB irons (e.g., Wasson, 2013), and, L/LL chondrites with IVA irons (e.g., Anand et al., 2021c).

Both CAIs and magmatic iron meteorites attest to high-temperature conditions during the earliest stages of solar system evolution; albeit

Table 7
^{26}Al-^{26}Mg, ^{53}Mn-^{53}Cr and ^{182}Hf-^{182}W chronological data for aubrites, angrites, ureilites and ungrouped achondrites.

Primitive achondrite	$(^{53}Mn/^{55}Mn)_0$	2σ	Age (Ma)	2σ	$^{26}Al/^{26}Mg$	2σ	Age (Ma)	2σ	$(^{182}Hf/^{180}Hf)_0$	2σ	Age (Ma)	2σ	Ref
Aubrites													
External isochron from bulk aubrites	2.00E−06	5.0E−07	6.51	1.19									a
External isochron from bulk aubrites	2.55E−06	5.2E−07	5.21	1.00									b
Angrites													
D'Orbigny	3.24E-06	4E−08	3.93	0.07	3.98E−07	1.5E−08	5.14	0.04	7.15E−05	1.7E−06	4.54	0.30	c, d, e
Sahara 99555	2.82E-06	3.7E−07	4.67	0.66	3.64E−07	1.8E−08	5.23	0.05	6.87E−05	1.5E−06	5.05	0.28	f, d, e
NWA 1296									7.01E−05	2.8E−06	4.79	0.50	e
NWA 4590									4.63E−05	1.7E−06	10.12	0.46	e
NWA 4801									4.52E−05	1.6E−06	10.42	0.45	e
LEW 86010	1.25E-06	7E−08	9.01	0.29					4.80E−05	4.2E−06	9.65	1.08	g, e
NWA 2999/4931									5.43E−05	3.4E−06	8.07	0.78	e
Angra dos Reis									4.02E−05	2.4E−06	11.93	0.74	e
NWA 1670	2.85E-06	9.2E−07	4.61	1.49	5.92E−07	5.9E−08	4.72	0.10					f, d
Asuka 881394	3.85E-06	2.3E−07	3.01	0.31	1.28E−06	7E−08	3.91	0.06					h
External isochron from bulk angrites	3.16E-06	1.1E−07	4.06	0.18									i
Ureilites													
DaG 165	2.84E−06	0.11E−06	4.63	0.20									j
ALM-A	3.10E−06	1.10E−06	4.17	1.62									k
NWA 766	3.35E−06	4.1E−07	3.75	0.62									l
External isochron from bulk ureilites	6.02E−06	1.59E−06	0.62	1.25									m
Ungrouped achondrites													
NWA 6704/6693	2.59E-06	3.4E−07	5.13	0.66	3.15E−07	3.8E−08	5.38	0.12					n
NWA 2976					3.94E−07	1.6E−08	5.15	0.04					o
NWA 7325					3.03E−07	1.4E−08	5.42	0.05					p
Asuka 881394					1.48E−06	1.2E−07	3.75	0.08					q
Tafassasset	3.32E-06	1.6E−07	3.80	0.25					7.40E−05	7.0E−06	4.10	1.2	r, s
EC 002	4.76E-06	3.9E−07	1.88	0.42	8.89E−06	9E−08	1.87	0.01					t, u
NWA 11119					1.69E−06	9E−08	3.61	0.05					v

Ref: (a) Shukolyukov and Lugmair (2004) (b) Zhu et al. (2021b) (c) Glavin et al. (2004) (d) Schiller et al. (2015) (e) Kleine et al. (2012) (f) Sugiura et al. (2005) (g) Lugmair and Shukolyukov (1998) (h) Wadhwa et al. (2009) (i) Zhu et al. (2019b) (j) Goodrich et al. (2010) (k) Qin et al. (2010b) (l) Yamakawa et al. (2010) (m) Zhu et al. (2020b) (n) Sanborn et al. (2019) (o) Bouvier et al. (2011) (p) Koefoed et al. (2016) (q) Wimpenny et al. (2019) (r) Göpel et al. (2015) (s) Breton et al. (2015) (t) Anand et al. (2022) (u) Fang et al. (2022) (v) Srinivasan et al. (2018).

with the heat originating from different sources. CAIs represent material processed possibly due to its close proximity to the newly formed Sun. In contrast, metallic cores of planetesimals, now represented by iron meteorites, formed due to early planetary accretion and heating by the abundant short-lived isotope ^{26}Al. The age of both materials and their chemical compositions require an early phase of dust aggregation followed by planetesimal accretion. Due to their early formation in a hot environment, these oldest materials did not preserve primary or primitive chemical and mineralogical composition. They bear evidence of strong element fractionation in high energy environments that erased most information on the primary elemental composition of the solar nebula from which they originated. However, these old materials preserve the isotopic compositions of their primary source in their bulk composition, which attest to strong isotope variability in the solar system at an early stage (e.g., Warren, 2011).

The early stages of the planetary system evolution are illustrated by direct observations of protoplanetary disks (e.g., Long et al., 2018) that show heterogeneous occurrence of matter in rings with different reflectivity. The accretion of the first planetesimals could have led to the formation of these gaps in the accretionary disks. The gaps between the dust rings are the feeding zones of the oldest planetesimals. Material cannot cross these gaps easily as they inhibit the radial transport of dust and gas (e.g., Alibert et al., 2018). This formation of early barriers to material transport prevented homogenization of the solar nebula and is preserved in the heterogeneous isotope compositions (i.e., nucleosynthetic anomalies) observed in the different meteorite classes (e.g., Warren, 2011). Early formed bodies i.e., Jupiter and the parent bodies of the oldest iron meteorites could have formed by streaming instabilities within the evolving solar nebula (e.g., Dullemond and Dominik, 2005; Ormel et al., 2010; B. Liu et al., 2019) followed by planetesimal collisions. Based on a comparison of the isotope composition of Earth and Mars with that of carbonaceous chondrites from the outer solar system, it has been suggested such an accretion model for the rocky planets of the inner solar system may represent the first mechanism of planetesimal accretion (e.g., Burkhardt et al., 2021).

The chemically most primitive or undifferentiated meteorites are chondrites, and they postdate the formation of many iron meteorites and all CAIs. One of their key components is chondrules which originated as high-temperature melts that cooled rapidly. Almost all silicate-dominated chondrules formed ca 1.8–3 Ma after CAIs, i.e., after three half-lives of ^{26}Al. Chondrules in ordinary chondrites may be slightly older than carbonaceous chondrites (Fig. 2). Ages determined on enstatite chondrites have generally higher uncertainties, thus their temporal relationship to chondrules from ordinary and carbonaceous chondrites are less clear. The metal-rich chondrules in CB meteorites formed later, ca. 4–5 Ma after CAIs. The subsequent accretion of silicate chondrules into different chondrite parent bodies was late enough (e.g., Anand et al., 2021a; Trieloff et al., 2003) to prevent planetesimal-wide

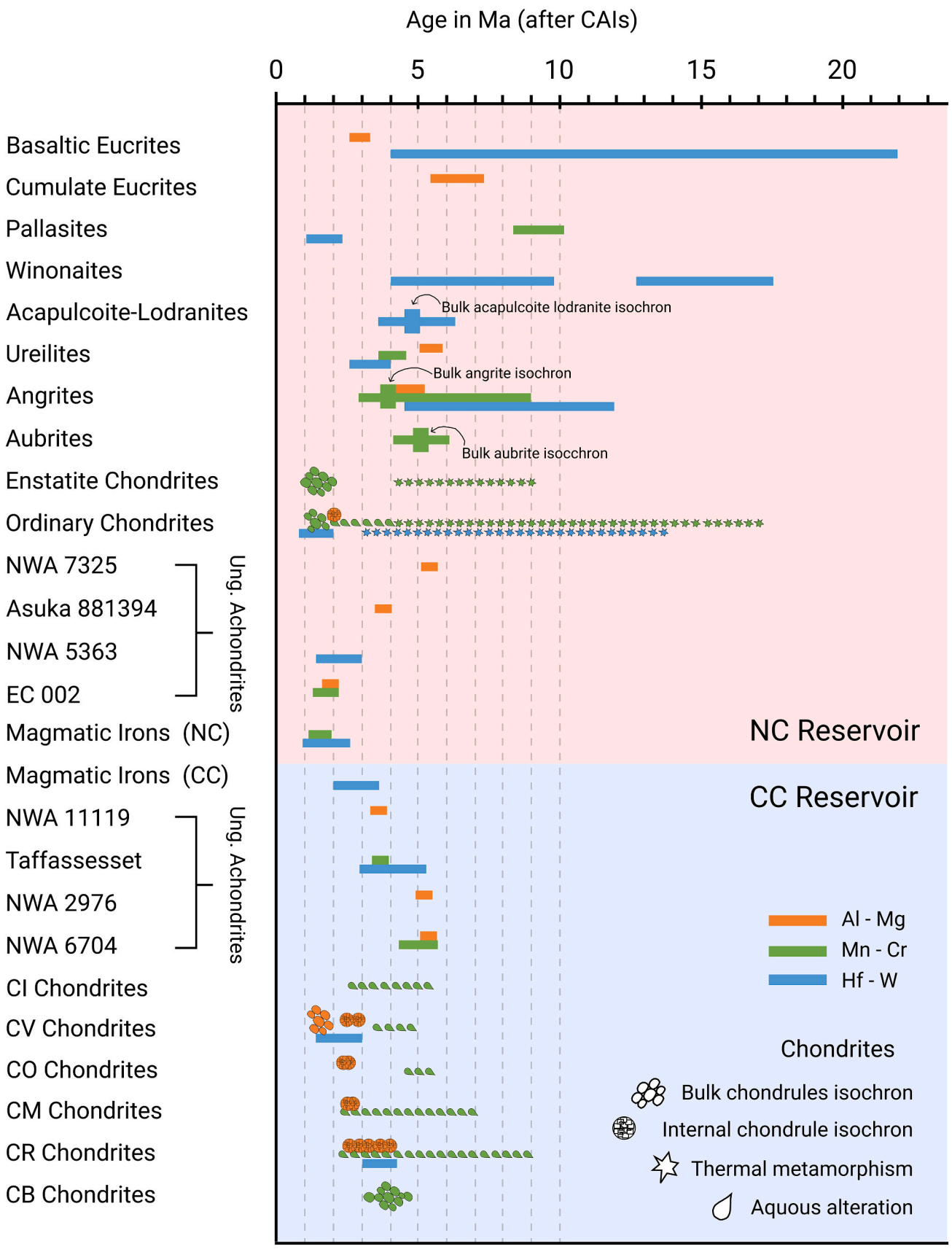

Fig. 7. A timeline of the events and processes in the early solar system from the time of CAI formation (t_0) to the accretion of the first large planetesimals.

melting and formation of metal cores, which allowed the preservation of the chondrule texture and the chemically primitive composition of chondrites.

Different high-temperature processes have been suggested as the cause for chondrule formation, including, the collision of planetesimals (e.g., Lichtenberg et al., 2018), heating by nebular shocks (e.g., Desch and Connolly Jr, 2002), or lightning (Horanyi et al., 1995). The observation that the extant chondrules are younger than the oldest planetesimals can be interpreted as evidence that early formed bodies were instrumental in chondrule formation. Early formed bodies that still needed to settle into stable orbits could have created bow shocks in the adjacent region still composed of dust and gas (e.g., Tsiganis et al., 2005; Morbidelli and Raymond, 2016; Bodénan et al., 2020b). It has been suggested that the giant planet Jupiter accreted prior to the chondrule forming interval (Kruijer et al., 2017). The shocks created by the migration of this large body and possibly the smaller planetesimals can have led to the melting of accreted dust agglomerations to form chondrules. This migration of Jupiter and the consequences for planet formation has been discussed extensively in the "grand tack models" (e.g., Raymond and Morbidelli, 2014). Chondrule formation by the collision of early formed and differentiated bodies is an unlikely process for chemically primitive chondrites, as mixing highly differentiated material (metal and silicates) to achieve again a chemically primitive, i.e., chondritic composition is difficult. However, the metal-rich chondrules found in CB meteorites could be the result of planetesimal collisions (e.g., Lichtenberg et al., 2018).

The chondrule-forming process is still enigmatic. The observation that chondrules formed relatively late and after the first planetesimals had accreted and differentiated into metal core and silicate mantle supports models that include early planetesimal formation as the cause rather than the result of chondrule formation. Chondrule formation is thus not a necessary step in planetary accretion, but rather a consequence of it. Chondrite parent bodies can be seen as a second generation of planetesimals, whereas the iron meteorites represent remnants of a first generation.

The accretion time of the different planetesimals cannot be dated directly using radio-isotopes. However, ages for thermal metamorphism and hydrous alteration can provide minimum ages and youngest chondrule formation ages can constrain the maximum ages for the chondrite parent-body accretion. Using the age systematics of ordinary chondrites, it can be shown that they accreted at ca. 3 Ma (Anand et al., 2021a). Aqueous alteration on carbonaceous chondrite parent bodies implies accretion before ca. 4 Ma (Table 3, Fig. 7).

The accretion ages estimated for chondrite parent bodies (e.g., Anand et al., 2021a; Trieloff et al., 2003, Fig. 7) are similar to the ages of their youngest chondrules, supporting a sudden accretion of chondrules and dust into a second generation of planetesimals. If there is a causal relationship between chondrule formation and planetesimals accretion, this close temporal relationship is consistent with the pebble accretion model proposed to explain the rapid accretion of planetary bodies (Cuzzi et al., 2008; Lambrechts and Johansen, 2012; Johansen and Lambrechts, 2017). This second planetesimal growth mechanism via pebble accretion may have been possible only after chondrule formation.

The accretion of hydrous material to carbonaceous chondrites is recorded in secondary minerals (e.g., carbonates, magnetite, fayalite and kirschsteinite) that formed by the interaction of water/ice with chondritic material. At least the physio-chemical conditions (temperature, water/rock ratio, pH, f_{O2}, and fluid compositions) in the outer regions of planetesimals must be suitable (e.g., Zolensky et al., 2008), for these reactions to take place at $\sim 4 \pm 2$ Ma, which also marks the end of major planetesimal accretion in the solar system, the disappearance of the solar nebula and the completion of accretion of Mars at ca. 5 Ma (Dauphas and Pourmand, 2011).

The accretion of the chondrite parent bodies after >4 half-lives of ^{26}Al and their relatively small size prevented planetesimal-wide melting and metal core formation thus preserving their chemically primitive composition. Members of the OCs show metamorphic grades from 3 to 7, whereas CCs are generally unmetamorphosed (except CKs that have petrologic types from 3 to 6). This difference in thermal evolution correlates with the later accretion of the CC parent bodies compared to the OC parent bodies. These differences are also in agreement with ^{26}Al being a major source for planetesimal heating, but only in the first few Ma of the solar system.

Silicate-dominated achondrites yield ages that are almost exclusively younger than 4 Ma after CAI. A rare exception is EC 002, which is the oldest known felsic rock from the solar system and has a crystallization age of 1.87 ± 0.01 Ma (Barrat et al., 2021; Fang et al., 2022; Anand et al., 2022). The crystallization of this meteorite coincides with the beginning of the chondrule-forming episode. The younger ages obtained for achondrites constrain mineral growth due to high-grade metamorphism or melting in large bodies like Vesta or the angrite and ureilite parent bodies. These late high-temperature processes were caused by impact accretion and/or decay of remaining ^{26}Al in bodies large enough that heat production was faster than heat loss by conduction.

A key observation from the age compilation is that processes and events in the early solar system do not follow an identical timeline from dust to planetesimal formation and they do not correlate with the location in the disk. Similar processes occurred at different times in different locations. It is likely that a radial temperature gradient existed in the early solar system disk at the time of dust formation and planetesimal accretion. However, this continuous gradient was not a dominant factor controlling the accretion process. It did not have a strong effect on the chemical composition of the accreting material and the timing of accretion into planetesimals. There is an indication that processes like first metal core formation, chondrule formation and accretion of chondrite parent bodies occurred slightly later (a few 10^5a) in the CC than in the NC reservoir. Thus, accretion from dust to planets was a sequence of spatially and temporally punctuated events rather than events and processes that swept over time from the inner to the outer region of the solar disk or vice versa following a unique timeline. The compilation of ages from primitive and differentiated meteorites shows that planetesimal formation was essentially completed in the first 4 Ma of the existence of the solar system, using the oldest CAIs as definition as the start, or t_0.

Declaration of competing interest

The authors declare that they have no known competing financial interests or personal relationships that could have appeared to influence the work reported in this paper.

Acknowledgements

This study was partially funded by the 'Swiss Government Excellence Scholarship (2018.0371)'. We acknowledge funding within the framework of the NCCR PlanetS supported by the Swiss National Science Foundation grant no. 51NF40-141881. We thank the two anonymous reviewers for their constructive and extensive comments that led to substantial improvements of the paper.

References

Alibert, Y., Venturini, J., Helled, R., Ataiee, S., Burn, R., Senecal, L., Benz, W., Mayer, L., Mordasini, C., Quanz, S.P., Schönbächler, M., 2018. The formation of Jupiter by hybrid pebble-planetesimal accretion. Nat. Astron. 2 (11), 873–877.

Amelin, Y., 2006. The prospect of high-precision Pb isotopic dating of meteorites. Meteorit. Planet. Sci. 41 (1), 7–17.

Amelin, Y., Kaltenbach, A., Iizuka, T., Stirling, C.H., Ireland, T.R., Petaev, M., Jacobsen, S.B., 2010. U–Pb chronology of the Solar System's oldest solids with variable ^{238}U/^{235}U. Earth Planet. Sci. Lett. 300 (3–4), 343–350.

Anand, A., Pape, J., Wille, M., Mezger, K., 2021a. Chronological constraints on the thermal evolution of ordinary chondrite parent bodies from the ^{53}Mn-^{53}Cr system. Geochim. Cosmochim. Acta 307, 281–301.

Anand, A., Pape, J., Wille, M., Mezger, K., Hofmann, B.A., 2021b. Early differentiation of magmatic iron meteorite parent bodies from Mn–Cr chronometry. Geochem. Perspect. Lett. 20, 6–10.
Anand, A., Pape, J., Mezger, K., Hofmann, B., 2021c. Cr and O Isotopes Link IVA Irons and LL Chondrites (Abstract #6154). LPI Contribution 2609.
Anand, A., Kruttasch, P.M., Mezger, K., 2022. ^{53}Mn-^{53}Cr chronology and ε^{54}Cr-Δ^{17}O genealogy of Erg Chech 002: the oldest andesite in the solar system. Meteorit. Planet. Sci. 57 (11), 2003–2016.
Baker, J.A., Schiller, M., Bizzarro, M., 2012. ^{26}Al–^{26}Mg deficit dating ultramafic meteorites and silicate planetesimal differentiation in the early Solar System? Geochim. Cosmochim. Acta 77, 415–431.
Barrat, J.A., Chaussidon, M., Yamaguchi, A., Beck, P., Villeneuve, J., Byrne, D.J., Broadley, M.W., Marty, B., 2021. A 4,565-My-old andesite from an extinct chondritic protoplanet. Proc. Natl. Acad. Sci. 118 (11), e2026129118.
Becker, H., Walker, R.J., 2003. In search of extant Tc in the early solar system: ^{98}Ru and ^{99}Ru abundances in iron meteorites and chondrites. Chem. Geol. 196 (1–4), 43–56.
Bischoff, A., Alexander, C.M.D., Barrat, J.A., Burkhardt, C., Busemann, H., Degering, D., Di Rocco, T., Fischer, M., Fockenberg, T., Foustoukos, D.I., Gattacceca, J., 2021. The old, unique C1 chondrite Flensburg–insight into the first processes of aqueous alteration, brecciation, and the diversity of water-bearing parent bodies and lithologies. Geochimica et Cosmochimica Acta 293, 142–186.
Bizzarro, M., Baker, J.A., Haack, H., 2004. Mg isotope evidence for contemporaneous formation of chondrules and refractory inclusions. Nature 431 (7006), 275–278.
Bodénan, J.D., Starkey, N.A., Russell, S.S., Wright, I.P., Franchi, I.A., 2020a. One of the earliest refractory inclusions and its implications for solar system history. Geochim. Cosmochim. Acta 286, 214–226.
Bodénan, J.D., Surville, C., Szulágyi, J., Mayer, L., Schönbächler, M., 2020b. Can chondrules be produced by the interaction of Jupiter with the protosolar disk? Astrophys. J. 901 (1), 60.
Bollard, J., Connelly, J.N., Bizzarro, M., 2015. Pb-Pb dating of individual chondrules from the CB a chondrite Gujba: assessment of the impact plume formation model. Meteorit. Planet. Sci. 50 (7), 1197–1216.
Bollard, J., Connelly, J.N., Whitehouse, M.J., Pringle, E.A., Bonal, L., Jørgensen, J.K., Nordlund, Å., Moynier, F., Bizzarro, M., 2017. Early formation of planetary building blocks inferred from Pb isotopic ages of chondrules. Sci. Adv. 3 (8), e1700407.
Bollard, J., Kawasaki, N., Sakamoto, N., Olsen, M., Itoh, S., Larsen, K., Wielandt, D., Schiller, M., Connelly, J.N., Yurimoto, H., Bizzarro, M., 2019. Combined U-corrected Pb-Pb dating and ^{26}Al-^{26}Mg systematics of individual chondrules–evidence for a reduced initial abundance of ^{26}Al amongst inner Solar System chondrules. Geochim. Cosmochim. Acta 260, 62–83.
Bouvier, A., Spivak-Birndorf, L.J., Brennecka, G.A., Wadhwa, M., 2011. New constraints on early Solar System chronology from Al–Mg and U–Pb isotope systematics in the unique basaltic achondrite Northwest Africa 2976. Geochim. Cosmochim. Acta 75 (18), 5310–5323.
Brennecka, G.A., Kleine, T., 2017. A low abundance of ^{135}Cs in the early Solar System from barium isotopic signatures of volatile-depleted meteorites. Astrophys. J. Lett. 837 (1), L9.
Brennecka, G.A., Wadhwa, M., 2012. Uranium isotope compositions of the basaltic angrite meteorites and the chronological implications for the early Solar System. Proc. Natl. Acad. Sci. 109 (24), 9299–9303.
Brennecka, G.A., Borg, L.E., Romaniello, S.J., Souders, A.K., Shollenberger, Q.R., Marks, N.E., Wadhwa, M., 2017. A renewed search for short-lived ^{126}Sn in the early Solar System: hydride generation MC-ICPMS for high sensitivity Te isotopic analysis. Geochim. Cosmochim. Acta 201, 331–344.
Breton, T., Quitté, G., Toplis, M.J., Monnereau, M., Birck, J.L., Göpel, C., Charles, C., 2015. Tafassasset: evidence of early incipient differentiation on a metal-rich chondritic parent body. Earth Planet. Sci. Lett. 425, 193–203.
Budde, G., Kruijer, T.S., Fischer-Gödde, M., Irving, A.J., Kleine, T., 2015. Planetesimal differentiation revealed by the Hf–W systematics of ureilites. Earth Planet. Sci. Lett. 430, 316–325.
Budde, G., Burkhardt, C., Brennecka, G.A., Fischer-Gödde, M., Kruijer, T.S., Kleine, T., 2016a. Molybdenum isotopic evidence for the origin of chondrules and a distinct genetic heritage of carbonaceous and non-carbonaceous meteorites. Earth Planet. Sci. Lett. 454, 293–303.
Budde, G., Kleine, T., Kruijer, T.S., Burkhardt, C., Metzler, K., 2016b. Tungsten isotopic constraints on the age and origin of chondrules. Proc. Natl. Acad. Sci. 113 (11), 2886–2891.
Budde, G., Kruijer, T.S., Kleine, T., 2018. Hf-W chronology of CR chondrites: implications for the timescales of chondrule formation and the distribution of ^{26}Al in the solar nebula. Geochim. Cosmochim. Acta 222, 284–304.
Burkhardt, C., Kleine, T., Oberli, F., Pack, A., Bourdon, B., Wieler, R., 2011. Molybdenum isotope anomalies in meteorites: constraints on solar nebula evolution and origin of the Earth. Earth Planet. Sci. Lett. 312 (3–4), 390–400.
Burkhardt, C., Dauphas, N., Tang, H., Fischer-Gödde, M., Qin, L., Chen, J.H., Rout, S.S., Pack, A., Heck, P.R., Papanastassiou, D.A., 2017. In search of the Earth-forming reservoir: mineralogical, chemical, and isotopic characterizations of the ungrouped achondrite NWA 5363/NWA 5400 and selected chondrites. Meteorit. Planet. Sci. 52 (5), 807–826.
Burkhardt, C., Dauphas, N., Hans, U., Bourdon, B., Kleine, T., 2019. Elemental and isotopic variability in solar system materials by mixing and processing of primordial disk reservoirs. Geochim. Cosmochim. Acta 261, 145–170.
Burkhardt, C., Spitzer, F., Morbidelli, A., Budde, G., Render, J.H., Kruijer, T.S., Kleine, T., 2021. Terrestrial planet formation from lost inner solar system material. Sci. Adv. 7 (52), eabj7601.
Chaussidon, M., Robert, F., McKeegan, K.D., 2006. Li and B isotopic variations in an Allende CAI: evidence for the in-situ decay of short-lived ^{10}Be and for the possible presence of the short-lived nuclide ^{7}Be in the early solar system. Geochim. Cosmochim. Acta 70 (1), 224–245.
Connelly, J.N., Bizzarro, M., Krot, A.N., Nordlund, A., 2012. The absolute chronology and thermal processing of solids in the solar protoplanetary disk. Science 338, 651–655.
Connolly, H.C., Zipfel, J., Folco, L., Smith, C., Jones, R.H., Benedix, G., Righter, K., Yamaguchi, A., Chennaoui, Aoudjehane H., Grossman, J.N., 2007. The meteoritical bulletin, No. 91, 2007 March. Meteorit. Planet. Sci. 42, 413–466.
Cuzzi, J.N., Hogan, R.C., Shariff, K., 2008. Toward planetesimals: Dense chondrule clumps in the protoplanetary nebula. The Astrophys. J. 687 (2), 1432.
Dauphas, N., Pourmand, A., 2011. Hf–W–Th evidence for rapid growth of Mars and its status as a planetary embryo. Nature 473 (7348), 489–492.
Davis, A.M., 2022. Short-lived nuclides in the early solar system: abundances, origins, and applications. Annu. Rev. Nucl. Part. Sci. 72, 339–363.
deLeuw, S., Rubin, A.E., Schmitt, A.K., Wasson, J.T., 2009. ^{53}Mn–^{53}Cr systematics of carbonates in CM chondrites: implications for the timing and duration of aqueous alteration. Geochim. Cosmochim. Acta 73 (24), 7433–7442.
Desch, S.J., Connolly Jr., H., 2002. A model of the thermal processing of particles in solar nebula shocks: application to the cooling rates of chondrules. Meteorit. Planet. Sci. 37 (2), 183–207.
Desch, S.J., Kalyaan, A., Alexander, C.M., O'D, 2018. The effect of Jupiter's formation on the distribution of refractory elements and inclusions in meteorites. Astrophys. J. Suppl. Ser. 238 (1), 11.
Doyle, P.M., Jogo, K., Nagashima, K., Krot, A.N., Wakita, S., Ciesla, F.J., Hutcheon, I.D., 2015. Early aqueous activity on the ordinary and carbonaceous chondrite parent bodies recorded by fayalite. Nat. Commun. 6 (1), 1–10.
Dullemond, C.P., Dominik, C., 2005. Dust coagulation in protoplanetary disks: a rapid depletion of small grains. Astron. Astrophys. 434, 971–986.
Dunham, E.T., Wadhwa, M., Desch, S.J., Liu, M.C., Fukuda, K., Kita, N., Hertwig, A.T., Hervig, R.L., Defouilloy, C., Simon, S.B., Davidson, J., 2022. Uniform initial ^{10}Be/^{9}Be inferred from refractory inclusions in CV3, CO3, CR2, and CH/CB chondrites. Geochim. Cosmochim. Acta 324, 194–220.
Endress, M., Zinner, E., Bischoff, A., 1996. Early aqueous activity on primitive meteorite parent bodies. Nature 379 (6567), 701–703.
Fahey, A.J., Goswami, J.N., McKeegan, K.D., Zinner, E., 1987. ^{26}Al, ^{244}Pu, ^{50}Ti, REE, and trace element abundances in hibonite grains from CM and CV meteorites. Geochim. Cosmochim. Acta 51 (2), 329–350.
Fang, L., Frossard, P., Boyet, M., Bouvier, A., Barrat, J.A., Chaussidon, M., Moynier, F., 2022. Half-life and initial Solar System abundance of ^{146}Sm determined from the oldest andesitic meteorite. Proc. Natl. Acad. Sci. 119 (12), e2120933119.
Friedman, A.M., Milsted, J., Metta, D., Henderson, D., Lerner, J., Harkness, A.L., Op, D. R., 1966. Alpha decay half-lives of ^{148}Gd ^{150}Gd and ^{146}Sm. Radiochim. Acta 5 (4), 192–194.
Fujiya, W., Sugiura, N., Hotta, H., Ichimura, K., Sano, Y., 2012. Evidence for the late formation of hydrous asteroids from young meteoritic carbonates. Nat. Commun. 3 (1), 1–6.
Fujiya, W., Sugiura, N., Sano, Y., Hiyagon, H., 2013. Mn–Cr ages of dolomites in CI chondrites and the Tagish Lake ungrouped carbonaceous chondrite. Earth Planet. Sci. Lett. 362, 130–142.
Fukuda, K., Tenner, T.J., Kimura, M., Tomioka, N., Siron, G., Ushikubo, T., Chaumard, N., Hertwig, A.T., Kita, N.T., 2022. A temporal shift of chondrule generation from the inner to outer Solar System inferred from oxygen isotopes and Al-Mg chronology of chondrules from primitive CM and CO chondrites. Geochim. Cosmochim. Acta 322, 194–226.
Galy, A., Young, E.D., Ash, R.D., Keith O'Nions, R., 2000. The formation of chondrules at high gas pressures in the solar nebula. Science 290 (5497), 1751–1753.
Glavin, D.P., Kubny, A., Jagoutz, E., Lugmair, G.W., 2004. Mn-Cr isotope systematics of the D'Orbigny angrite. Meteorit. Planet. Sci. 39 (5), 693–700.
Goldstein, J.I., Scott, E.R.D., Chabot, N.L., 2009. Iron meteorites: crystallization, thermal history, parent bodies, and origin. Geochemistry 69 (4), 293–325.
Goodrich, C.A., Scott, E.R., Fioretti, A.M., 2004. Ureilitic breccias: clues to the petrologic structure and impact disruption of the ureilite parent asteroid. Geochemistry 64 (4), 283–327.
Goodrich, C.A., Hutcheon, I.D., Kita, N.T., Huss, G.R., Cohen, B.A., Keil, K., 2010. ^{53}Mn–^{53}Cr and ^{26}Al–^{26}Mg ages of a feldspathic lithology in polymict ureilites. Earth Planet. Sci. Lett. 295 (3–4), 531–540.
Goodrich, C.A., Kita, N.T., Yin, Q.Z., Sanborn, M.E., Williams, C.D., Nakashima, D., Lane, M.D., Boyle, S., 2017. Petrogenesis and provenance of ungrouped achondrite Northwest Africa 7325 from petrology, trace elements, oxygen, chromium and titanium isotopes, and mid-IR spectroscopy. Geochim. Cosmochim. Acta 203, 381–403.
Göpel, C., Birck, J.L., Galy, A., Barrat, J.A., Zanda, B., 2015. Mn–Cr systematics in primitive meteorites: insights from mineral separation and partial dissolution. Geochim. Cosmochim. Acta 156, 1–24.
Guan, Y., Huss, G.R., Leshin, L.A., 2007. ^{60}Fe–^{60}Ni and ^{53}Mn–^{53}Cr isotopic systems in sulfides from unequilibrated enstatite chondrites. Geochim. Cosmochim. Acta 71 (16), 4082–4091.
Haba, M.K., Lai, Y.J., Wotzlaw, J.F., Yamaguchi, A., Lugaro, M., Schönbächler, M., 2021. Precise initial abundance of Niobium-92 in the Solar System and implications for p-process nucleosynthesis. Proc. Natl. Acad. Sci. 118 (8), e2017750118.
Han, J., Keller, L.P., Liu, M.C., Needham, A.W., Hertwig, A.T., Messenger, S., Simon, J.I., 2020. A coordinated microstructural and isotopic study of a Wark-Lovering rim on a Vigarano CAI. Geochim. Cosmochim. Acta 269, 639–660.
Heck, P.R., Greer, J., Kööp, L., Trappitsch, R., Gyngard, F., Busemann, H., Maden, C., Ávila, J.N., Davis, A.M., Wieler, R., 2020. Lifetimes of interstellar dust from cosmic

ray exposure ages of presolar silicon carbide. Proc. Natl. Acad. Sci. 117 (4), 1884–1889.
Hellmann, J.L., Kruijer, T.S., Van Orman, J.A., Metzler, K., Kleine, T., 2019. Hf-W chronology of ordinary chondrites. Geochim. Cosmochim. Acta 258, 290–309.
Hellmann, J.L., Kruijer, T.S., Metzler, K., Patzek, M., Pack, A., Berndt, J., Kleine, T., 2020. Hf-W chronology of a macrochondrule from the L5/6 chondrite Northwest Africa 8192. Meteorit. Planet. Sci. 55 (10), 2241–2255.
Hellmann, J.L., Walker, R.J., 2023. Hf-W isotope systematics of bulk chondrites: Implications for iron meteorite model ages. Lunar Planet. Sci. Conf. 54.
Hertwig, A.T., Kimura, M., Ushikubo, T., Defouilloy, C., Kita, N.T., 2019. The ^{26}Al-^{26}Mg systematics of FeO-rich chondrules from Acfer 094: two chondrule generations distinct in age and oxygen isotope ratios. Geochim. Cosmochim. Acta 253, 111–126.
Hilton, C.D., Bermingham, K.R., Walker, R.J., McCoy, T.J., 2019. Genetics, crystallization sequence, and age of the South Byron trio iron meteorites: new insights to carbonaceous chondrite (CC) type parent bodies. Geochim. Cosmochim. Acta 251, 217–228.
Hopp, J., Storck, J.C., Ludwig, T., Mostefaoui, S., Altherr, R., Ott, U., Meyer, H.P., Trieloff, M., 2021. ^{53}Mn-^{53}Cr systematics of sphalerite in enstatite chondrites. Geochim. Cosmochim. Acta 310, 79–94.
Hoppe, P., Zinner, E., 2000. Presolar dust grains from meteorites and their stellar sources. J. Geophys. Res. Space Physics 105 (A5), 10371–10385.
Hoppe, P., MacDougall, D., Lugmair, G.W., 2007. High spatial resolution ion microprobe measurements refine chronology of carbonate formation in Orgueil. Meteorit. Planet. Sci. 42 (7–8), 1309–1320.
Horanyi, M., Morfill, G., Goertz, C.K., Levy, E.H., 1995. Chondrule formation in lightning discharges. Icarus 114 (1), 174–185.
Hua, X., Huss, G.R., Tachibana, S., Sharp, T.G., 2005. Oxygen, silicon, and Mn-Cr isotopes of fayalite in the Kaba oxidized CV3 chondrite: constraints for its formation history. Geochim. Cosmochim. Acta 69 (5), 1333–1348.
Hublet, G., Debaille, V., Wimpenny, J., Yin, Q.Z., 2017. Differentiation and magmatic activity in Vesta evidenced by ^{26}Al-^{26}Mg dating in eucrites and diogenites. Geochim. Cosmochim. Acta 218, 73–97.
Hutcheon, I.D., Hutchison, R., 1989. Evidence from the Semarkona ordinary chondrite for ^{26}A1 heating of small planets. Nature 337 (6204), 238–241.
Hutcheon, I.D., Jones, R.H., 1995. The ^{26}Al-^{26}Mg record of chondrules: clues to nebular chronology. In: Lunar and Planetary Science Conference, vol. 26.
Hutcheon, I.D., Krot, A.N., Keil, K., Phinney, D.L., Scott, E.R., 1998. ^{53}Mn-^{53}Cr dating of fayalite formation in the CV3 chondrite Mokoia: evidence for asteroidal alteration. Science 282 (5395), 1865–1867.
Ireland, T.R., 1988. Correlated morphological, chemical, and isotopic characteristics of hibonites from the Murchison carbonaceous chondrite. Geochim. Cosmochim. Acta 52 (12), 2827–2839.
Ireland, T.R., 1990. Presolar isotopic and chemical signatures in hibonite-bearing refractory inclusions from the Murchison carbonaceous chondrite. Geochim. Cosmochim. Acta 54 (11), 3219–3237.
Ireland, T.R., 1991. The abundances of ^{182}Hf in the early solar system. In: Lunar and Planetary Science Conference, vol. 22.
Ireland, T.R., Compston, W., 1987. Large heterogeneous ^{26}Mg excesses in a hibonite from the Murchison meteorite. Nature 327 (6124), 689–692.
Ireland, T.R., Zinner, E.K., Fahey, A.J., Esat, T.M., 1992. Evidence for distillation in the formation of HAL and related hibonite inclusions. Geochim. Cosmochim. Acta 56 (6), 2503–2520.
Jacobsen, B., Yin, Q.Z., Moynier, F., Amelin, Y., Krot, A.N., Nagashima, K., Hutcheon, I. D., Palme, H., 2008. ^{26}Al–^{26}Mg and ^{207}Pb–^{206}Pb systematics of Allende CAIs: canonical solar initial ^{26}Al/^{27}Al ratio reinstated. Earth Planet. Sci. Lett. 272 (1–2), 353–364.
Jilly, C.E., Huss, G.R., Krot, A.N., Nagashima, K., Yin, Q.Z., Sugiura, N., 2014. ^{53}Mn-^{53}Cr dating of aqueously formed carbonates in the CM2 lithology of the Sutter's Mill carbonaceous chondrite. Meteorit. Planet. Sci. 49 (11), 2104–2117.
Jilly-Rehak, C.E., Huss, G.R., Nagashima, K., 2017. ^{53}Mn–^{53}Cr radiometric dating of secondary carbonates in CR chondrites: timescales for parent body aqueous alteration. Geochim. Cosmochim. Acta 201, 224–244.
Jogo, K., Nakamura, T., Noguchi, T., Zolotov, M.Y., 2009. Fayalite in the Vigarano CV3 carbonaceous chondrite: occurrences, formation age and conditions. Earth Planet. Sci. Lett. 287 (3–4), 320–328.
Jogo, K., Nakamura, T., Ito, M., Wakita, S., Zolotov, M.Y., Messenger, S.R., 2017. Mn–Cr ages and formation conditions of fayalite in CV3 carbonaceous chondrites: constraints on the accretion ages of chondritic asteroids. Geochim. Cosmochim. Acta 199, 58–74.
Johansen, A., Lambrechts, M., 2017. Forming planets via pebble accretion. Annu. Rev. Earth Planet. Sci. 45, 359–387.
Kawasaki, N., Kato, C., Itoh, S., Wakaki, S., Ito, M., Yurimoto, H., 2015. ^{26}Al–^{26}Mg chronology and oxygen isotope distributions of multiple melting for a Type C CAI from Allende. Geochim. Cosmochim. Acta 169, 99–114.
Kawasaki, N., Simon, S.B., Grossman, L., Sakamoto, N., Yurimoto, H., 2018. Crystal growth and disequilibrium distribution of oxygen isotopes in an igneous Ca-Al-rich inclusion from the Allende carbonaceous chondrite. Geochim. Cosmochim. Acta 221, 318–341.
Kawasaki, N., Park, C., Sakamoto, N., Park, S.Y., Kim, H.N., Kuroda, M., Yurimoto, H., 2019. Variations in initial ^{26}Al/^{27}Al ratios among fluffy Type A Ca–Al-rich inclusions from reduced CV chondrites. Earth Planet. Sci. Lett. 511, 25–35.
Kawasaki, N., Wada, S., Park, C., Sakamoto, N., Yurimoto, H., 2020. Variations in initial ^{26}Al/^{27}Al ratios among fine-grained Ca-Al-rich inclusions from reduced CV chondrites. Geochim. Cosmochim. Acta 279, 1–15.
Kita, N.T., Ushikubo, T., 2012. Evolution of protoplanetary disk inferred from ^{26}Al chronology of individual chondrules. Meteorit. Planet. Sci. 47 (7), 1108–1119.
Kita, N.T., Nagahara, H., Togashi, S., Morishita, Y., 2000. A short duration of chondrule formation in the solar nebula: evidence from ^{26}Al in Semarkona ferromagnesian chondrules. Geochim. Cosmochim. Acta 64 (22), 3913–3922.
Kita, N.T., Huss, G.R., Tachibana, S., Amelin, Y., Nyquist, L., Hutcheon, I.D., 2005. Constraints on the Origin of Chondrules and CAIs From Short-lived and Long-lived Radionuclides.
Kita, N.T., Ushikubo, T., Knight, K.B., Mendybaev, R.A., Davis, A.M., Richter, F.M., Fournelle, J.H., 2012. Internal ^{26}Al–^{26}Mg isotope systematics of a Type B CAI: remelting of refractory precursor solids. Geochim. Cosmochim. Acta 86, 37–51.
Kita, N.T., Yin, Q.Z., MacPherson, G.J., Ushikubo, T., Jacobsen, B., Nagashima, K., Kurahashi, E., Krot, A.N., Jacobsen, S.B., 2013. ^{26}Al-^{26}Mg isotope systematics of the first solids in the early solar system. Meteorit. Planet. Sci. 48 (8), 1383–1400.
Kleine, T., Mezger, K., Palme, H., Münker, C., 2004. The W isotope evolution of the bulk silicate Earth: constraints on the timing and mechanisms of core formation and accretion. Earth Planet. Sci. Lett. 228, 109–123.
Kleine, T., Mezger, K., Palme, H., Scherer, E., Münker, C., 2005. Early core formation in asteroids and late accretion of chondrite parent bodies: evidence from ^{182}Hf-^{182}W in CAIs, metal-rich chondrites, and iron meteorites. Geochim. Cosmochim. Acta 69 (24), 5805–5818.
Kleine, T., Touboul, M., Bourdon, B., Nimmo, F., Mezger, K., Palme, H., Jacobsen, S.B., Yin, Q.Z., Halliday, A.N., 2009. Hf–W chronology of the accretion and early evolution of asteroids and terrestrial planets. Geochim. Cosmochim. Acta 73 (17), 5150–5188.
Kleine, T., Hans, U., Irving, A.J., Bourdon, B., 2012. Chronology of the angrite parent body and implications for core formation in protoplanets. Geochim. Cosmochim. Acta 84, 186–203.
Koefoed, P., Amelin, Y., Yin, Q.Z., Wimpenny, J., Sanborn, M.E., Iizuka, T., Irving, A.J., 2016. U–Pb and Al–Mg systematics of the ungrouped achondrite Northwest Africa 7325. Geochim. Cosmochim. Acta 183, 31–45.
Koike, M., Sugiura, N., Takahata, N., Ishida, A., Sano, Y., 2017. U-Pb and Hf-W dating of young zircon in mesosiderite Asuka 882023. Geophys. Res. Lett. 44 (3), 1251–1259.
Kööp, L., Davis, A.M., Nakashima, D., Park, C., Krot, A.N., Nagashima, K., Tenner, T.J., Heck, P.R., Kita, N.T., 2016a. A link between oxygen, calcium and titanium isotopes in ^{26}Al-poor hibonite-rich CAIs from Murchison and implications for the heterogeneity of dust reservoirs in the solar nebula. Geochim. Cosmochim. Acta 189, 70–95.
Kööp, L., Nakashima, D., Heck, P.R., Kita, N.T., Tenner, T.J., Krot, A.N., Nagashima, K., Park, C., Davis, A.M., 2016b. New constraints on the relationship between ^{26}Al and oxygen, calcium, and titanium isotopic variation in the early Solar System from a multielement isotopic study of spinel-hibonite inclusions. Geochim. Cosmochim. Acta 184, 151–172.
Kööp, L., Nakashima, D., Heck, P.R., Kita, N.T., Tenner, T.J., Krot, A.N., Nagashima, K., Park, C., Davis, A.M., 2018. A multielement isotopic study of refractory FUN and F CAIs: Mass-dependent and mass-independent isotope effects. Geochim. Cosmochim. Acta 221, 296–317.
Krot, A.N., 2019. Refractory inclusions in carbonaceous chondrites: records of early solar system processes. Meteorit. Planet. Sci. 54 (8), 1647–1691.
Krot, A.N., Amelin, Y., Cassen, P., Meibom, A., 2005. Young chondrules in CB chondrites from a giant impact in the early Solar System. Nature 436 (7053), 989–992.
Krot, A.N., Makide, K., Nagashima, K., Huss, G.R., Ogliore, R.C., Ciesla, F.J., Yang, L., Hellebrand, E., Gaidos, E., 2012. Heterogeneous distribution of ^{26}Al at the birth of the solar system: evidence from refractory grains and inclusions. Meteorit. Planet. Sci. 47 (12), 1948–1979.
Kruijer, T.S., Kleine, T., Fischer-Gödde, M., Burkhardt, C., Wieler, R., 2014a. Nucleosynthetic W isotope anomalies and the Hf-W chronometry of Ca-Al-rich inclusions. Earth Planet. Sci. Lett. 403, 317–327.
Kruijer, T.S., Touboul, M., Fischer-Gödde, M., Bermingham, K.R., Walker, R.J., Kleine, T., 2014b. Protracted core formation and rapid accretion of protoplanets. Science 344 (6188), 1150–1154.
Kruijer, T.S., Burkhardt, C., Budde, G., Kleine, T., 2017. Age of Jupiter inferred from the distinct genetics and formation times of meteorites. Proc. Natl. Acad. Sci. 114 (26), 6712–6716.
Kruijer, T.S., Burkhardt, C., Borg, L.E., Kleine, T., 2022. Tungsten and molybdenum isotopic evidence for an impact origin of pallasites. Earth Planet. Sci. Lett. 584, 117440.
Kunihiro, T., Rubin, A.E., McKeegan, K.D., Wasson, J.T., 2004. Initial ^{26}Al/^{27}Al in carbonaceous-chondrite chondrules: too little ^{26}Al to melt asteroids. Geochim. Cosmochim. Acta 68 (13), 2947–2957.
Kurahashi, E., Kita, N.T., Nagahara, H., Morishita, Y., 2008. ^{26}Al-^{26}Mg systematics of chondrules in a primitive CO chondrite. Geochim. Cosmochim. Acta 72 (15), 3865–3882.
Lambrechts, M., Johansen, A., 2012. Rapid growth of gas-giant cores by pebble accretion. Astron. Astrophys. 544, A32.
Larsen, K.K., Trinquier, A., Paton, C., Schiller, M., Wielandt, D., Ivanova, M.A., Connelly, J.N., Nordlund, Å., Krot, A.N., Bizzarro, M., 2011. Evidence for magnesium isotope heterogeneity in the solar protoplanetary disk. Astrophys. J. Lett. 735 (2), L37.
Larsen, K.K., Wielandt, D., Schiller, M., Krot, A.N., Bizzarro, M., 2020. Episodic formation of refractory inclusions in the Solar System and their presolar heritage. Earth Planet. Sci. Lett. 535, 116088.
Lee, D.C., Halliday, A.N., 2000. Accretion of primitive planetesimals: Hf-W isotopic evidence from enstatite chondrites. Science 288 (5471), 1629–1631.
Lichtenberg, T., Golabek, G.J., Dullemond, C.P., Schönbächler, M., Gerya, T.V., Meyer, M.R., 2018. Impact splash chondrule formation during planetesimal recycling. Icarus 302, 27–43.

Liu, M.C., McKeegan, K.D., Goswami, J.N., Marhas, K.K., Sahijpal, S., Ireland, T.R., Davis, A.M., 2009. Isotopic records in CM hibonites: implications for timescales of mixing of isotope reservoirs in the solar nebula. Geochim. Cosmochim. Acta 73 (17), 5051–5079.
Liu, M.C., Chaussidon, M., Srinivasan, G., McKeegan, K.D., 2012. A lower initial abundance of short-lived ^{41}Ca in the early solar system and its implications for solar system formation. Astrophys. J. 761 (2), 137.
Liu, B., Ormel, C.W., Johansen, A., 2019a. Growth after the streaming instability-from planetesimal accretion to pebble accretion. Astron. Astrophys. 624, A114.
Liu, M.C., Han, J., Brearley, A.J., Hertwig, A.T., 2019b. Aluminum-26 chronology of dust coagulation and early solar system evolution. Sci. Adv. 5 (9), eaaw3350.
Long, F., Pinilla, P., Herczeg, G.J., Harsono, D., Dipierro, G., Pascucci, I., Hendler, N., Tazzari, M., Ragusa, E., Salyk, C., Edwards, S., 2018. Gaps and rings in an ALMA Survey of disks in the Taurus star-forming region. Astrophys. J. 869 (1), 17.
Lugmair, G.W., Shukolyukov, A., 1998. Early solar system timescales according to ^{53}Mn-^{53}Cr systematics. Geochim. Cosmochim. Acta 62 (16), 2863–2886.
Luu, T.H., Young, E.D., Gounelle, M., Chaussidon, M., 2015. Short time interval for condensation of high-temperature silicates in the solar accretion disk. Proc. Natl. Acad. Sci. 112 (5), 1298–1303.
Luu, T.H., Hin, R.C., Coath, C.D., Elliott, T., 2019. Bulk chondrite variability in mass independent magnesium isotope compositions–implications for initial solar system ^{26}Al/^{27}Al and the timing of terrestrial accretion. Earth Planet. Sci. Lett. 522, 166–175.
MacPherson, G.J., Bullock, E.S., Janney, P.E., Kita, N.T., Ushikubo, T., Davis, A.M., Wadhwa, M., Krot, A.N., 2010. Early solar nebula condensates with canonical, not supracanonical, initial ^{26}Al/^{27}Al ratios. Astrophys. J. Lett. 711 (2), L117.
MacPherson, G.J., Kita, N.T., Ushikubo, T., Bullock, E.S., Davis, A.M., 2012. Well-resolved variations in the formation ages for Ca–Al-rich inclusions in the early Solar System. Earth Planet. Sci. Lett. 331, 43–54.
MacPherson, G.J., Bullock, E.S., Tenner, T.J., Nakashima, D., Kita, N.T., Ivanova, M.A., Krot, A.N., Petaev, M.I., Jacobsen, S.B., 2017a. High precision Al–Mg systematics of forsterite-bearing Type B CAIs from CV3 chondrites. Geochim. Cosmochim. Acta 201, 65–82.
MacPherson, G.J., Nagashima, K., Krot, A.N., Doyle, P.M., Ivanova, M.A., 2017b. ^{53}Mn–^{53}Cr chronology of Ca–Fe silicates in CV3 chondrites. Geochim. Cosmochim. Acta 201, 260–274.
MacPherson, G.J., Defouilloy, C., Kita, N.T., 2018. High-precision Al–Mg isotopic systematics in USNM 3898–the benchmark "ALL" for initial ^{87}Sr/^{86}Sr in the earliest Solar System. Earth Planet. Sci. Lett. 491, 238–243.
MacPherson, G.J., Krot, A.N., Nagashima, K., 2020. Al-Mg isotopic study of spinel-rich fine-grained CAIs. Meteorit. Planet. Sci. 55 (11), 2519–2538.
MacPherson, G.J., Krot, A.N., Kita, N.T., Bullock, E.S., Nagashima, K., Ushikubo, T., Ivanova, M.A., 2022. The formation of Type B CAIs: evolution from Type A CAIs. Geochim. Cosmochim. Acta 321, 343–374.
Makide, K., Nagashima, K., Krot, A.N., Huss, G.R., Ciesla, F.J., Hellebrand, E., Gaidos, E., Yang, L., 2011. Heterogeneous distribution of ^{26}Al at the birth of the solar system. Astrophys. J. Lett. 733 (2), L31.
Makide, K., Nagashima, K., Krot, A.N., Huss, G.R., Hutcheon, I.D., Hellebrand, E., Petaev, M.I., 2013. Heterogeneous distribution of ^{26}Al at the birth of the Solar System: evidence from corundum-bearing refractory inclusions in carbonaceous chondrites. Geochim. Cosmochim. Acta 110, 190–215.
Mane, P., Wallace, S., Bose, M., Wallace, P., Wadhwa, M., Weber, J., Zega, T.J., 2022. Earliest evidence of nebular shock waves recorded in a calcium-aluminum-rich inclusion. Geochim. Cosmochim. Acta 332, 369–388.
Marrocchi, Y., Piralla, M., Regnault, M., Batanova, V., Villeneuve, J., Jacquet, E., 2022. Isotopic evidence for two chondrule generations in CR chondrites and their relationships to other carbonaceous chondrites. Earth Planet. Sci. Lett. 593, 117683.
McCain, K.A., Matsuda, N., Liu, M.C., McKeegan, K.D., Yamaguchi, A., Kimura, M., Tomioka, N., Ito, M., Imae, N., Uesugi, M., Shirai, N., 2023. Early fluid activity on Ryugu inferred by isotopic analyses of carbonates and magnetite. Nature Astronomy 1–9.
Meissner, F., Schmidt-Ott, W.D., Ziegeler, L., 1987. Half-life and α-ray energy of ^{146}Sm. Z. Phys. A Atomic Nuclei 327 (2), 171–174.
Mishra, R.K., Chaussidon, M., 2014. Timing and extent of Mg and Al isotopic homogenization in the early inner Solar System. Earth Planet. Sci. Lett. 390, 318–326.
Mishra, R.K., Goswami, J.N., Tachibana, S., Huss, G.R., Rudraswami, N.G., 2010. ^{60}Fe and ^{26}Al in chondrules from unequilibrated chondrites: implications for early solar system processes. Astrophys. J. Lett. 714 (2), L217.
Morbidelli, A., Raymond, S.N., 2016. Challenges in planet formation. J. Geophys. Res. Planets 121 (10), 1962–1980.
Mostefaoui, S., Kita, N.T., Togashi, S., Tachibana, S., Nagahara, H., Morishita, Y., 2002. The relative formation ages of ferromagnesian chondrules inferred from their initial aluminum-26/aluminum-27 ratios. Meteorit. Planet. Sci. 37 (3), 421–438.
Nagashima, K., Krot, A.N., Chaussidon, M., 2007. Aluminum-magnesium isotope systematics of chondrules from CR chondrites. Meteorit. Planet. Sci. Suppl. 42, 5291.
Nagashima, K., Krot, A.N., Huss, G.R., 2008. ^{26}Al in chondrules from CR carbonaceous chondrites. In: 39th Annual Lunar and Planetary Science Conference, p. 2224 (No. 1391.
Nagashima, K., Krot, A.N., Huss, G.R., 2014. ^{26}Al in chondrules from CR2 chondrites. Geochem. J. 48 (6), 561–570.
Nagashima, K., Krot, A.N., Komatsu, M., 2017. ^{26}Al–^{26}Mg systematics in chondrules from Kaba and Yamato 980145 CV3 carbonaceous chondrites. Geochim. Cosmochim. Acta 201, 303–319.
Nakamura, E., Kobayashi, K., Tanaka, R., Kunihiro, T., Kitagawa, H., Potiszil, C., Ota, T., Sakaguchi, C., Yamanaka, M., Ratnayake, D.M., Tripathi, H., 2022. On the origin and evolution of the asteroid Ryugu: A comprehensive geochemical perspective. Proc. Japan Acad. Ser. B 98 (6), 227–282.
Neuland, M.B., Mezger, K., Riedo, A., Tulej, M., Wurz, P., 2021. The chemical composition and homogeneity of the Allende matrix. Planet. Space Sci. 204, 105251.
Neumann, W., Breuer, D., Spohn, T., 2012. Differentiation and core formation in accreting planetesimals. Astron. Astrophys. 543, A141.
Nishiizumi, K., 2004. Preparation of ^{26}Al AMS standards. Nucl. Instrum. Methods Phys. Res., Sect. B 223, 388–392.
Nyquist, L.E., Kleine, T., Shih, C.Y., Reese, Y.D., 2009. The distribution of short-lived radioisotopes in the early solar system and the chronology of asteroid accretion, differentiation, and secondary mineralization. Geochim. Cosmochim. Acta 73 (17), 5115–5136.
Ormel, C.W., Dullemond, C.P., Spaans, M., 2010. Accretion among preplanetary bodies: The many faces of runaway growth. Icarus 210 (1), 507–538.
Palk, E., Andreasen, R., Rehkämper, M., Stunt, A., Kreissig, K., Coles, B., Schönbächler, M., Smith, C., 2018. Variable Tl, Pb, and Cd concentrations and isotope compositions of enstatite and ordinary chondrites-evidence for volatile element mobilization and decay of extinct ^{205}Pb. Meteorit. Planet. Sci. 53 (2), 167–186.
Pape, J., Mezger, K., Bouvier, A.S., Baumgartner, L.P., 2019. Time and duration of chondrule formation: constraints from ^{26}Al-^{26}Mg ages of individual chondrules. Geochim. Cosmochim. Acta 244, 416–436.
Pape, J., Rosén, Å.V., Mezger, K., Guillong, M., 2021. Primary crystallization and partial remelting of chondrules in the protoplanetary disk: petrographic, mineralogical and chemical constraints recorded in zoned type-I chondrules. Geochim. Cosmochim. Acta 292, 499–517.
Park, C., Nagashima, K., Krot, A.N., Huss, G.R., Davis, A.M., Bizzarro, M., 2017. Calcium-aluminum-rich inclusions with fractionation and unidentified nuclear effects (FUN CAIs): II. Heterogeneities of magnesium isotopes and ^{26}Al in the early Solar System inferred from in situ high-precision magnesium-isotope measurements. Geochim. Cosmochim. Acta 201, 6–24.
Pellas, P., Storzer, D., 1981. ^{244}Pu fission track thermometry and its application to stony meteorites. Proc. R. Soc. Lond. A Math. Phys. Sci. 374 (1757), 253–270.
Petitat, M., Marrocchi, Y., McKeegan, K.D., Mostefaoui, S., Meibom, A., Zolensky, M.E., Gounelle, M., 2011. ^{53}Mn-^{53}Cr ages of Kaidun carbonates. Meteorit. Planet. Sci. 46 (2), 275–283.
Qin, L., Alexander, C.M.D., Carlson, R.W., Horan, M.F., Yokoyama, T., 2010a. Contributors to chromium isotope variation of meteorites. Geochim. Cosmochim. Acta 74 (3), 1122–1145.
Qin, L., Rumble, D., Alexander, C.M.O.D., Carlson, R.W., Jenniskens, P., Shaddad, M.H., 2010b. The chromium isotopic composition of Almahata Sitta. Meteorit. Planet. Sci. 45 (10−11), 1771–1777.
Raymond, S.N., Morbidelli, A., 2014. The Grand Tack model: A critical review. Proc. Inter. Astro. Union 9 (S310), 194–203.
Reger, P.M., Roebbert, Y., Neumann, W., Gannoun, A., Regelous, M., Schwarz, W.H., Ludwig, T., Trieloff, M., Weyer, S., Bouvier, A., 2023. Al-Mg and U-Pb chronological records of Erg Chech 002 ungrouped achondrite meteorite. Geochim. Cosmochim. Acta 343, 33–48.
Roszjar, J., Whitehouse, M.J., Srinivasan, G., Mezger, K., Scherer, E.E., Van Orman, J.A., Bischoff, A., 2016. Prolonged magmatism on 4 Vesta inferred from Hf–W analyses of eucrite zircon. Earth Planet. Sci. Lett. 452, 216–226.
Rudraswami, N.G., Goswami, J.N., 2007. ^{26}Al in chondrules from unequilibrated L chondrites: onset and duration of chondrule formation in the early solar system. Earth Planet. Sci. Lett. 257 (1–2), 231–244.
Rudraswami, N.G., Goswami, J.N., Chattopadhyay, B., Sengupta, S.K., Thapliyal, A.P., 2008. ^{26}Al records in chondrules from unequilibrated ordinary chondrites: II. Duration of chondrule formation and parent body thermal metamorphism. Earth Planet. Sci. Lett. 274 (1–2), 93–102.
Sahijpal, S., Goswami, J.N., Davis, A.M., 2000. K, Mg, Ti and Ca isotopic compositions and refractory trace element abundances in hibonites from CM and CV meteorites: implications for early solar system processes. Geochim. Cosmochim. Acta 64 (11), 1989–2005.
Sanborn, M.E., Wimpenny, J., Williams, C.D., Yamakawa, A., Amelin, Y., Irving, A.J., Yin, Q.Z., 2019. Carbonaceous achondrites Northwest Africa 6704/6693: milestones for early Solar System chronology and genealogy. Geochim. Cosmochim. Acta 245, 577–596.
Sanders, I.S., Scott, E.R., 2022. Complementary nucleosynthetic isotope anomalies of Mo and W in chondrules and matrix in the Allende carbonaceous chondrite: the case for hydrothermal metamorphism and its implications. Meteorit. Planet. Sci. 57 (2), 450–471.
Schiller, M., Baker, J.A., Bizzarro, M., 2010a. ^{26}Al–^{26}Mg dating of asteroidal magmatism in the young Solar System. Geochim. Cosmochim. Acta 74 (16), 4844–4864.
Schiller, M., Handler, M.R., Baker, J.A., 2010b. High-precision Mg isotopic systematics of bulk chondrites. Earth Planet. Sci. Lett. 297 (1–2), 165–173.
Schiller, M., Connelly, J.N., Glad, A.C., Mikouchi, T., Bizzarro, M., 2015. Early accretion of protoplanets inferred from a reduced inner solar system ^{26}Al inventory. Earth Planet. Sci. Lett. 420, 45–54.
Schönbächler, M., Carlson, R.W., Horan, M.F., Mock, T.D., Hauri, E.H., 2008. Silver isotope variations in chondrites: volatile depletion and the initial ^{107}Pd abundance of the solar system. Geochim. Cosmochim. Acta 72 (21), 5330–5341.
Schrader, D.L., Nagashima, K., Krot, A.N., Ogliore, R.C., Yin, Q.Z., Amelin, Y., Stirling, C. H., Kaltenbach, A., 2017. Distribution of ^{26}Al in the CR chondrite chondrule-forming region of the protoplanetary disk. Geochim. Cosmochim. Acta 201, 275–302.
Schulz, T., Münker, C., Mezger, K., Palme, H., 2010. Hf-W chronometry of primitive achondrites. Geochim. Cosmochim. Acta 74, 1706–1718.

Scott, E.R., Sanders, I.S., 2009. Implications of the carbonaceous chondrite Mn–Cr isochron for the formation of early refractory planetesimals and chondrules. Geochim. Cosmochim. Acta 73 (17), 5137–5149.
Shukolyukov, A., Lugmair, G.W., 2004. Manganese-chromium isotope systematics of enstatite meteorites. Geochim. Cosmochim. Acta 68 (13), 2875–2888.
Shukolyukov, A., Lugmair, G.W., 2006. Manganese–chromium isotope systematics of carbonaceous chondrites. Earth Planet. Sci. Lett. 250 (1–2), 200–213.
Simon, S.B., Krot, A.N., Nagashima, K., 2019. Oxygen and Al-Mg isotopic compositions of grossite-bearing refractory inclusions from CO 3 chondrites. Meteorit. Planet. Sci. 54 (6), 1362–1378.
Siron, G., Fukuda, K., Kimura, M., Kita, N.T., 2021. New constraints from ^{26}Al-^{26}Mg chronology of anorthite bearing chondrules in unequilibrated ordinary chondrites. Geochim. Cosmochim. Acta 293, 103–126.
Siron, G., Fukuda, K., Kimura, M., Kita, N.T., 2022. High precision ^{26}Al-^{26}Mg chronology of chondrules in unequilibrated ordinary chondrites: evidence for restricted formation ages. Geochim. Cosmochim. Acta 324, 312–345.
Spitzer, F., Burkhardt, C., Nimmo, F., Kleine, T., 2021. Nucleosynthetic Pt isotope anomalies and the Hf-W chronology of core formation in inner and outer solar system planetesimals. Earth Planet. Sci. Lett. 576, 117211.
Spivak-Birndorf, L., Wadhwa, M., Janney, P., 2009. ^{26}Al–^{26}Mg systematics in D'Orbigny and Sahara 99555 angrites: implications for high-resolution chronology using extinct chronometers. Geochim. Cosmochim. Acta 73 (17), 5202–5211.
Srinivasan, P., Dunlap, D.R., Agee, C.B., Wadhwa, M., Coleff, D., Ziegler, K., Zeigler, R., McCubbin, F.M., 2018. Silica-rich volcanism in the early solar system dated at 4.565 Ga. Nat. Commun. 9 (1), 1–8.
Sugiura, N., Fujiya, W., 2014. Correlated accretion ages and ε^{54}Cr of meteorite parent bodies and the evolution of the solar nebula. Meteorit. Planet. Sci. 49 (5), 772–787.
Sugiura, N., Hoshino, H., 2003. Mn-Cr chronology of five IIIAB iron meteorites. Meteorit. Planet. Sci. 38 (1), 117–143.
Sugiura, N., Krot, A.N., 2007. ^{26}Al-^{26}Mg systematics of Ca-Al-rich inclusions, amoeboid olivine aggregates, and chondrules from the ungrouped carbonaceous chondrite Acfer 094. Meteorit. Planet. Sci. 42 (7–8), 1183–1195.
Sugiura, N., Miyazaki, A., Yanai, K., 2005. Widespread magmatic activities on the angrite parent body at 4562 Ma ago. Earth Planets Space 57 (9), e13–e16.
Suttle, M.D., King, A.J., Schofield, P.F., Bates, H., Russell, S.S., 2021. The aqueous alteration of CM chondrites, a review. Geochim. Cosmochim. Acta 299, 219–256.
Tang, H., Dauphas, N., 2015. Low ^{60}Fe abundance in Semarkona and Sahara 99555. Astrophys. J. 802 (1), 22.
Tang, H., Liu, M.C., McKeegan, K.D., Tissot, F.L., Dauphas, N., 2017. In situ isotopic studies of the U-depleted Allende CAI Curious Marie: pre-accretionary alteration and the co-existence of ^{26}Al and ^{36}Cl in the early solar nebula. Geochim. Cosmochim. Acta 207, 1–18.
Tenner, T.J., Nakashima, D., Ushikubo, T., Tomioka, N., Kimura, M., Weisberg, M.K., Kita, N.T., 2019. Extended chondrule formation intervals in distinct physicochemical environments: evidence from Al-Mg isotope systematics of CR chondrite chondrules with unaltered plagioclase. Geochim. Cosmochim. Acta 260, 133–160.
Tissot, F.L., Dauphas, N., Grossman, L., 2016. Origin of uranium isotope variations in early solar nebula condensates. Sci. Adv. 2 (3), e1501400.
Tissot, F.L., Dauphas, N., Grove, T.L., 2017. Distinct ^{238}U/^{235}U ratios and REE patterns in plutonic and volcanic angrites: geochronologic implications and evidence for U isotope fractionation during magmatic processes. Geochim. Cosmochim. Acta 213, 593–617.
Tornabene, H.A., Hilton, C.D., Bermingham, K.R., Ash, R.D., Walker, R.J., 2020. Genetics, age and crystallization history of group IIC iron meteorites. Geochim. Cosmochim. Acta 288, 36–50.
Tornabene, H.A., Ash, R.D., Walker, R.J., Bermingham, K.R., 2023. Genetics, age, and crystallization history of group IC iron meteorites. Geochim. Cosmochim. Acta 340, 108–119.
Touboul, M., Kleine, T., Bourdon, B., Van Orman, J.A., Maden, C., Zipfel, J., 2009. Hf–W thermochronometry: II. Accretion and thermal history of the acapulcoite–lodranite parent body. Earth Planet. Sci. Lett. 284 (1–2), 168–178.
Touboul, M., Sprung, P., Aciego, S.M., Bourdon, B., Kleine, T., 2015. Hf–W chronology of the eucrite parent body. Geochim. Cosmochim. Acta 156, 106–121.
Trieloff, M., Jessberger, E.K., Herrwerth, I., Hopp, J., Fiéni, C., Ghélis, M., Bourot-Denise, M., Pellas, P., 2003. Structure and thermal history of the H-chondrite parent asteroid revealed by thermochronometry. Nature 422 (6931), 502–506.
Trinquier, A., Birck, J.L., Allègre, C.J., Göpel, C., Ulfbeck, D., 2008. ^{53}Mn–^{53}Cr systematics of the early Solar System revisited. Geochim. Cosmochim. Acta 72 (20), 5146–5163.
Tsiganis, K., Gomes, R., Morbidelli, A., Levison, H.F., 2005. Origin of the orbital architecture of the giant planets of the Solar System. Nature 435 (7041), 459–461.
Turner, G., Busfield, A., Crowther, S.A., Harrison, M., Mojzsis, S.J., Gilmour, J., 2007. Pu–Xe, U–Xe, U–Pb chronology and isotope systematics of ancient zircons from Western Australia. Earth Planet. Sci. Lett. 261 (3–4), 491–499.
Ushikubo, T., Kimura, M., Nakashima, D., Kita, N.T., 2010. A combined study of the Al-Mg systematics and O isotope ratios of chondrules from the primitive carbonaceous chondrite Acfer 094. In: 41st Annual Lunar and Planetary Science Conference, p. 1491 (No. 1533).
Ushikubo, T., Nakashima, D., Kimura, M., Tenner, T.J., Kita, N.T., 2013. Contemporaneous formation of chondrules in distinct oxygen isotope reservoirs. Geochim. Cosmochim. Acta 109, 280–295.
Ushikubo, T., Tenner, T.J., Hiyagon, H., Kita, N.T., 2017. A long duration of the ^{16}O-rich reservoir in the solar nebula, as recorded in fine-grained refractory inclusions from the least metamorphosed carbonaceous chondrites. Geochim. Cosmochim. Acta 201, 103–122.
Van Schmus, W.R., Wood, J.A., 1967. A chemical-petrologic classification for the chondritic meteorites. Geochim. Cosmochim. Acta 31 (5), 747–765.
Villeneuve, J., Chaussidon, M., Libourel, G., 2009. Homogeneous distribution of ^{26}Al in the solar system from the Mg isotopic composition of chondrules. Science 325 (5943), 985–988.
Visser, R., John, T., Whitehouse, M.J., Patzek, M., Bischoff, A., 2020. A short-lived ^{26}Al induced hydrothermal alteration event in the outer solar system: constraints from Mn/Cr ages of carbonates. Earth Planet. Sci. Lett. 547, 116440.
Wada, S., Kawasaki, N., Park, C., Yurimoto, H., 2020. Melilite condensed from an ^{16}O-poor gaseous reservoir: evidence from a fine-grained Ca-Al-rich inclusion of Northwest Africa 8613. Geochim. Cosmochim. Acta 288, 161–175.
Wadhwa, M., Shukolyukov, A., Davis, A.M., Lugmair, G.W., Mittlefehldt, D.W., 2003. Differentiation history of the mesosiderite parent body: constraints from trace elements and manganese-chromium isotope systematics in Vaca Muerta silicate clasts. Geochim. Cosmochim. Acta 67 (24), 5047–5069.
Wadhwa, M., Amelin, Y., Bogdanovski, O., Shukolyukov, A., Lugmair, G.W., Janney, P., 2009. Ancient relative and absolute ages for a basaltic meteorite: implications for timescales of planetesimal accretion and differentiation. Geochim. Cosmochim. Acta 73 (17), 5189–5201.
Warren, P.H., 2011. Stable-isotopic anomalies and the accretionary assemblage of the Earth and Mars: a subordinate role for carbonaceous chondrites. Earth Planet. Sci. Lett. 311 (1–2), 93–100.
Warren, P.H., Ulff-Møller, F., Huber, H., Kallemeyn, G.W., 2006. Siderophile geochemistry of ureilites: a record of early stages of planetesimal core formation. Geochim. Cosmochim. Acta 70 (8), 2104–2126.
Wasserburg, G.J., Wimpenny, J., Yin, Q.Z., 2012. Mg isotopic heterogeneity, Al-Mg isochrons, and canonical ^{26}Al/^{27}Al in the early solar system. Meteorit. Planet. Sci. 47 (12), 1980–1997.
Wasson, J.T., 2013. Vesta and extensively melted asteroids: why HED meteorites are probably not from Vesta. Earth Planet. Sci. Lett. 381, 138–146.
White, W.M., 2023. Isotope Geochemistry. John Wiley & Sons.
Williams, C.D., Ushikubo, T., Bullock, E.S., Janney, P.E., Hines, R.R., Kita, N.T., Hervig, R.L., MacPherson, G.J., Mendybaev, R.A., Richter, F.M., Wadhwa, M., 2017. Thermal and chemical evolution in the early solar system as recorded by FUN CAIs: part I–petrology, mineral chemistry, and isotopic composition of Allende FUN CAI CMS-1. Geochim. Cosmochim. Acta 201, 25–48.
Wimpenny, J., Sanborn, M.E., Koefoed, P., Cooke, I.R., Stirling, C., Amelin, Y., Yin, Q.Z., 2019. Reassessing the origin and chronology of the unique achondrite Asuka 881394: implications for distribution of ^{26}Al in the early Solar System. Geochim. Cosmochim. Acta 244, 478–501.
Windmill, R.J., Franchi, I.A., Hellmann, J.L., Schneider, J.M., Spitzer, F., Kleine, T., Greenwood, R.C., Anand, M., 2022. Isotopic evidence for pallasite formation by impact mixing of olivine and metal during the first 10 million years of the Solar System. PNAS Nexus 1 (1), pgac015.
Yamakawa, A., Yamashita, K., Makishima, A., Nakamura, E., 2010. Chromium isotope systematics of achondrites: chronology and isotopic heterogeneity of the inner solar system bodies. Astrophys. J. 720 (1), 150.
Yamashita, K., Maruyama, S., Yamakawa, A., Nakamura, E., 2010. ^{53}Mn–^{53}Cr chronometry of CB chondrite: evidence for uniform distribution of ^{53}Mn in the early solar system. Astrophys. J. 723 (1), 20.
Yin, Q.Z., Jacobsen, B., Moynier, F., Hutcheon, I.D., 2007. Toward consistent chronology in the early solar system: high-resolution ^{53}Mn-^{53}Cr chronometry for chondrules. Astrophys. J. 662 (1), L43.
Yokoyama, T., et al., 2022. Samples returned from the asteroid Ryugu are similar to Ivuna-type carbonaceous meteorites. Science 379, eabn7850.
Yurimoto, H., Wasson, J.T., 2002. Extremely rapid cooling of a carbonaceous-chondrite chondrule containing very ^{16}O-rich olivine and a ^{26}Mg-excess. Geochim. Cosmochim. Acta 66 (24), 4355–4363.
Zhu, K., Liu, J., Moynier, F., Qin, L., Alexander, C.M.D., He, Y., 2019a. Chromium isotopic evidence for an early formation of chondrules from the Ornans CO chondrite. Astrophys. J. 873 (1), 82.
Zhu, K., Moynier, F., Wielandt, D., Larsen, K.K., Barrat, J.A., Bizzarro, M., 2019b. Timing and origin of the angrite parent body inferred from Cr isotopes. Astrophys. J. Lett. 877 (1), L13.
Zhu, K., Moynier, F., Schiller, M., Bizzarro, M., 2020a. Dating and tracing the origin of enstatite chondrite chondrules with Cr isotopes. Astrophys. J. Lett. 894 (2), L26.
Zhu, K., Moynier, F., Schiller, M., Wielandt, D., Larsen, K.K., van Kooten, E.M., Barrat, J. A., Bizzarro, M., 2020b. Chromium isotopic constraints on the origin of the ureilite parent body. Astrophys. J. 888 (2), 126.
Zhu, K., Moynier, F., Schiller, M., Alexander, C.M.D., Davidson, J., Schrader, D.L., van Kooten, E., Bizzarro, M., 2021a. Chromium isotopic insights into the origin of chondrite parent bodies and the early terrestrial volatile depletion. Geochim. Cosmochim. Acta 301, 158–186.
Zhu, K., Moynier, F., Schiller, M., Becker, H., Barrat, J.A., Bizzarro, M., 2021b. Tracing the origin and core formation of the enstatite achondrite parent bodies using Cr isotopes. Geochim. Cosmochim. Acta 308, 256–272.
Zolensky, M.E., Krot, A.N., Benedix, G., 2008. Record of low-temperature alteration in asteroids. Rev. Mineral. Geochem. 68 (1), 429–462.